APPLICATION OF SATELLITE-DERIVED WIND PROFILES TO JOINT PRECISION AIRDROP SYSTEM (JPADS) OPERATIONS

THESIS

David C. Meier, Major, USAF

AFIT/GAP/ENP/10-M10

DEPARTMENT OF THE AIR FORCE
AIR UNIVERSITY

AIR FORCE INSTITUTE OF TECHNOLOGY

Wright-Patterson Air Force Base, Ohio

AFIT/GAP/ENP/10-M10

APPLICATION OF SATELLITE-DERIVED WIND PROFILES TO JOINT PRECISION AIRDROP SYSTEM (JPADS) OPERATIONS

THESIS

Presented to the Faculty

Department of Engineering Physics

Graduate School of Engineering and Management

Air Force Institute of Technology

Air University

Air Education and Training Command

In Partial Fulfillment of the Requirements for the

Degree of Master of Science in Applied Physics

David C. Meier, BS

Major, USAF

March 2010

AFIT/GAP/ENP/10-M10

APPLICATION OF SATELLITE-DERIVED WIND PROFILES TO JOINT PRECISION AIRDROP SYSTEM (JPADS) OPERATIONS

David C. Meier, BS
Major, USAF

Approved:

Steven T. Fiorino, PhD (Chairman)	12 MAR 10 Date
Kevin C. Gross, PhD (Member)	15 MAR 10 Date
John F. Polander (Member)	22 MAR 10 Date

Abstract

The Joint Precision Airdrop System has revolutionized military airdrop capability, allowing accurate delivery of equipment and supplies to smaller drop zones, from higher altitudes than was previously possible. This capability depends on accurate wind data which is currently provided by a combination of high-resolution forecast models and GPS dropsondes released in the vicinity of the dropzone shortly before the airdrop. This research develops a windprofiling algorithm to derive the needed wind data from passive IR satellite soundings, eliminating the requirement for a hazardous dropsonde pass near the drop zone, or allowing the dropsonde to be dropped farther from the dropzone. Atmospheric temperature measurements made by the Atmospheric Infrared Sounder (AIRS) onboard the polar-orbiting Aqua satellite are gridded to create a three-dimensional temperature field surrounding a notional airdrop objective area. From these temperatures, pressure surfaces are calculated and geostrophic and thermal wind direction and magnitude are predicted for 25 altitudes between the surface and 500 mb level. These wind profiles are compared to rawinsonde measurements from balloon releases near the notional airdrop location and time of the satellite sounding. The validity of the satellite-derived wind profile is demonstrated at higher altitudes, but this method does not consistently predict wind velocity within the boundary layer. Future research which better accounts for surface friction may improve these results and lead to the single-pass airdrop capability desired by Air Mobility Command.

Acknowledgments

I would first like to express my sincere appreciation to my faculty advisor Dr. Steven Fiorino, for his guidance during this research effort. His expertise and enthusiastic approach toward the subject made the project enlightening and enjoyable. I would also like to thank committee members Dr. Kevin Gross and Mr. John Polander for insights and recommendations that were vital to the completion of this thesis

I am especially grateful to my wife for her patience and support throughout this project.

David C. Meier

Table of Contents

Page

Page

List of Figures

Figure Page

List of Tables

Table Page

APPLICATION OF SATELLITE-DERIVED WIND PROFILES TO JOINT PRECISION AIRDROP SYSTEM (JPADS) OPERATIONS

I. Introduction

Background

The Joint Precision Airdrop System was developed to provide airdrop capable aircraft the ability to carry out high altitude cargo airdrop with accuracy previously unattainable. The evolving system relies heavily on advancements in GPS guidance systems and parachute decelerators, but it was also made possible by an advanced computer based mission planning tool and rapid assimilation of weather data.

The JPADS system uses a high-resolution 4-D wind forecast provided by atmospheric models. This wind field is used for preflight mission planning, but alone it is not reliable enough for consistent, accurate high altitude airdrop. Aircrews need the ability to update the winds during flight prior to an airdrop to correct errors in the forecast model. As currently employed, this update is obtained by dropping a GPS dropsonde in the vicinity of the dropzone and receiving wind data by radio. The JPADS Mission Planner (JPADS-MP) incorporates the new wind profile and recalculates a computed air release point (CARP).

The updated CARP, displayed on the mission planner laptop, is verified by the aircrew and is manually entered into the aircraft's navigation system. Depending on the type of aircraft performing the mission, this task is accomplished by the navigator or by an additional crewmember referred to as the Precision Airdrop System (PADS) operator.

The crew is then prepared to return to the dropzone, configure the aircraft for airdrop, and navigate to the release point for the drop.

Dropsonde use for the wind update has proven effective, but is not the only possible method of obtaining a wind profile to update the JPADS-MP. Existing wind profile data computed from US GOES satellite soundings could be applied to high altitude JPADS operations in North America. Satellite sounding takes advantage of remote sensing techniques to measure the temperature of the atmosphere at multiple altitudes. From the temperature gradient, wind strength and direction at each level are derived. This wind profile could be used to update the JPADS-MP, eliminating the requirement for release of a dropsonde. A major drawback preventing operational use of this technique is the fact that the GOES satellite system only covers North America.

While the European METEOSAT system does not currently compute gradient winds from satellite sounding data, the available raw data can be processed to generate wind profiles for locations in Southwest Asia, enhancing the effectiveness and accuracy of operational airdrops in the current CENTCOM Area of Responsibility. This method will provide the capability for low cost, single-pass airdrop operations sought by Air Mobility Command.

Motivation

The Joint Precision Airdrop System was developed to utilize near real-time wind data for altitudes between the surface and drop altitude, and specialized, portable hardware components on an aircraft to compute a High Altitude Release Point (HARP). From this computed release point, GPS guided cargo systems are able to make glide path corrections to land very close to their intended point of impact on the ground.

Due to their high cost, the difficulty in returning the reusable components from the field, and the current requirement for frequent high-altitude combat airdrops; guided cargo systems are not available in sufficient quantities to meet demand. As these systems began to prove themselves, it was realized that the accurate wind profile received from a GPS dropsonde and the new JPADS mission planning software could allow a vast improvement in the accuracy of non-guided Container Delivery System (CDS) airdrops from medium altitudes (5,000-10,000 feet AGL). The process of dropping these non-guided ballistic parachute cargo systems from a JPADS-MP computed release point is referred to as Improved Container Delivery System (ICDS).

Air Mobility Command has embraced the ICDS method as the standard for CDS airdrops. In the combat environment, the risk to an aircraft is greatly increased if the mission requires flight over the same objective area twice, as is the case when a dropsonde is used to measure wind over the dropzone. To prevent the increased exposure of the aircraft in the threat environment and increased chance of compromising the location of friendly forces on the ground, AMC is pursuing alternatives to the dropsonde for wind measurement. The single pass airdrop is an important future capability which will be required for continued combat JPADS operations (Staine-Pyne, 2009).

Problem Statement

The current procedure for both guided JPADS and ICDS airdrops, according to the AMC Concept of Employment (CONEMP), requires airdrop of a GPS dropsonde within 25 nautical miles of the drop zone, a minimum of 20 minutes prior to the airdrop of cargo. This two-pass approach is effective, but is not optimal in a combat environment where accurate determination of ground threat locations is difficult. AMC is pursuing

multiple technologies that have the potential to eliminate the need for the first pass over the drop zone to release the dropsonde.

Options being considered fall into three categories, each with advantages and limitations. The ground-based solutions are to release a balloon, launch a rocket, or fly small unmanned aerial vehicle (UAV) from an area near the drop zone to determine the winds prior to the drop. These methods would be inexpensive, and could be implemented in the near future, but would require prepositioned equipment and training for the forces on the ground. Another challenge is that these ground-based solutions would rely on close coordination for mission changes that would affect the drop time.

The next category of proposed solutions does not eliminate the first pass, but allows it to be flown by a different aircraft from the cargo delivery aircraft. The aircraft delivering the dropsonde to the target location could be another aircraft from the same unit conducting the airdrop or could be a UAV, such as the Predator. The disadvantages of this solution are that it still requires two passes over the objective area, and requires the scheduling of a second aircraft for each airdrop.

The final category of solutions considered is platform-based wind sensing systems. High-resolution radar, LIDAR, or other optical systems could potentially measure wind ahead of and below the aircraft in real time providing data to compute and dynamically update a release point throughout the run-in to the airdrop, allowing for accurate cargo placement on the first pass. These are not near term solutions because it would be difficult to develop these to be portable, roll-on roll-off systems, and any needed aircraft modifications greatly increases the cost and time required. In addition, if the system computing the CARP is not directly tied into the aircraft's navigation system

presenting the release point to the pilots “under the glass”, the ability to react to last minute wind changes is lost. The current requirement for a navigator or PADS operator to manually verify and enter the release point coordinates in the aircraft’s computer after the JPADS-MP calculates it is the main reason the JPADS CONEMP requires 20 minutes from dropsonde release and cargo airdrop. Radar based methods have the problem of being less covert than other solutions. The emitted radar energy is detectable at a large distance, making aircraft detection in a combat environment easy for enemy forces. A disadvantage of the LIDAR and optical solutions is the inability to measure winds through significant clouds or rain.

An alternative approach, and the one investigated in this research, is to use satellite sounding data to compute a wind profile that can be used by the JPADS-MP to compute a CARP. This method only depends on passive satellite sounding, and has the potential to eliminate the need for the first aircraft pass over the drop zone. The wind profile computed could also be used in conjunction with any of the alternative wind measurement methods to validate their result or improve the CARP solution.

Theory

The process of computing a wind profile using satellite data begins with remote sensing brightness temperature at multiple locations and altitudes in the atmosphere. Passive vertical sounding measures the brightness temperature of the atmosphere, detecting the upwelling thermal radiation both from the surface and from the atmosphere itself. By selecting multiple channels in the vicinity of a strong absorption line of an atmospheric constituent gas, multiple values are measured--each corresponding to the temperature of a different layer of the atmosphere. Results are best if the absorption line

is for a gas which is well mixed throughout the troposphere and stratosphere, meaning its mass ratio is well known at all altitudes. Common gases used are oxygen and carbon dioxide (Petty, 2006).

The process of assigning temperature values to the measured radiances is an iterative process which finds the likely temperature profile and trace gas concentration that would have produced the observed set of measurements. The process begins with a guess at what the temperature profile might be and calculates the resulting weighting functions and radiances. These values are then compared with the observed values and the process repeated with a new initial temperature profile until convergence with the observation is achieved (Kidder and Vonder Haar, 1995).

This physical retrieval process and an algorithm to derive a wind profile from a satellite measured temperature field are described in detail in Chapter 2 of this document. Wind direction and velocity are not directly measured by this method, but are derived by applying physical principles to the temperature and pressure gradients. For this reason, there are more potential sources for error in this method than in the alternate method of computing winds from satellite observations, tracking cloud movement from subsequent images taken by geostationary satellites. Tracking clouds restricts useful wind calculation to altitudes where clouds are present. Clear air sounding, however, has the ability to derive winds simultaneously at multiple altitudes, providing the vertical profile needed to update the JPADS Mission Planner.

Research Approach

The first portion of this research analyzes the process currently in use to derive wind profiles from GOES satellite data, and develops a proof of concept algorithm to

compute similar wind fields using polar-orbiting satellite sounder data. The data available from the polar-orbiting satellites is compared to GOES and METEOSAT data, and the expected accuracy of wind data derived from the polar-orbiter data is evaluated.

Another goal of this research is to determine the applicability of these derived wind profiles for JPADS operations. Comparisons between satellite-derived winds and wind profiles obtained from GPS dropsondes will be made. Expected error in computed winds is analyzed in terms of the effect the error would have on CARP location and the ability to meet AMC requirements for JPADS airdrops.

The final phase of this research is recommendations for future research of possible strategies for combining satellite-derived winds with wind profiles from other sources (forecast model, GPS dropsonde, weather balloon, etc), and assess the advantage provided. The two specific approaches considered are how much improvement in accuracy can be obtained by incorporating satellite winds into wind profiles measured at the drop zone, and also how satellite-derived winds could be used in conjunction with a forecast model and winds measured 25-50 nautical miles away from the drop zone. This second use of the satellite data facilitates a single-pass airdrop, by calibrating the dropzone wind field generated by the forecast model. This potential application also depends on the terrain surrounding the drop zone—significant terrain between the objective area and location of wind measurement could lead to an unpredictable wind difference between the two.

Document Structure

Chapter 2 of this document is an overview of the JPADS program and a survey of existing research to summarize the current satellite remote temperature sensing

technology and wind field derivation, as well as how wind data is currently being used for JPADS operations. Chapter 3 outlines the methodology for each phase of this research. Chapter 4 details and analyzes the results obtained during each phase of research. The raw data currently available from satellite soundings is described, and an effective algorithm for processing this data to create usable wind profiles is defined. The final chapter, Chapter 5, summarizes the conclusions that can be drawn from this project. Recommendations are made for both appropriate use of satellite-derived winds, and areas for future research to improve their operational impact.

II. Literature Review

JPADS Program History

Development of the Joint Precision Airdrop System began in 1998 as a product of a partnership between AFRL, AMC and the US Army Soldier Systems Center. Initial efforts focused on leveraging technology to increase high altitude airdrop accuracy. Army Soldier Systems Center projects explored guided payload delivery vehicles. The USAF researched the technology needed to acquire near-real-time winds over the drop zone. The third area of research needed to lay the foundation of the USAF PADS program was capturing more accurate parachute ballistic characteristics to compute better release points and enable aerial delivery to smaller drop zones (AMC Single Pass Airdrop Workshop, 2009).

Over the following years, the Army advanced the guided payload delivery vehicles while the Air Force developed PADS software and the Mission Planner equipment. As these systems were reaching their first successful tests, the rapidly changing combat environments in Afghanistan and Iraq led CENTCOM to endorse Urgent Need Statements in both 2004 and 2006 requesting accelerated fielding the 2,000 pound JPADS payload delivery systems. In August 2006, ten prototype systems were delivered and by April 2007 over 60 systems were in place in the CENTCOM AOR (AMC Single Pass Airdrop Workshop, 2009).

JPADS Operations

The capabilities of the Joint Precision Airdrop System allow resupply of smaller tactical drop zones than previously possible from high altitude, providing critical flexibility to rapidly moving ground forces by the reducing the required DZ size. More

potential locations for dropzones are available, and the forces needed to secure the DZ are reduced. The increased accuracy minimizes the distance friendly ground forces need to travel in a combat environment to recover the cargo, and reduces the possibility that enemy forces intercept the cargo. Because the slow speed, straight and level flight profile required to execute a successful airdrop makes an aircraft especially vulnerable to attack from the ground, the ability to carry out these missions from higher altitudes, above many ground threat envelopes, reduces the risk to aircraft.

Richard Benney, JPADS Technical Manager at the US Army RD&E Command gives the following description of the current threat environment and its impact on the JPADS program. The proliferation of Man Portable Air Defense Systems (MANPADs) and other non-traditional threats presents a serious risk for airmen and soldiers conducting resupply operations. Supply line security is never guaranteed and insurgent forces are able to continually interdict the ground convoys that utilize them. There are significant risks and shortfalls associated with conducting conventional airdrop operations. For example, US and Allied Nation aircraft cannot meet desired accuracy standards once drop altitudes exceed 2000 feet above ground level (AGL). While drops below this altitude are more accurate, they are subject to small arms, Anti-Aircraft Artillery (AAA) and MANPAD threats. In addition, the time associated with deploying multiple payloads out of an aircraft necessitates a drop zone of substantial length for low altitude drops. Strategic, operational, and tactical employment of forces in the contemporary operating environment requires a change in the way US and Allied Nations sustain their forces. The time and place of the next battle is unknown and military planners are not able to define the next area of operations with certainty and thus can no

longer carefully prepare by strategic forward positioning of forces, equipment, and stocks. Current adversaries have developed tactics, techniques, and procedures that result in significant disruption of operations. Helicopters are downed by rocket-propelled grenades; vulnerable lines of communications are disrupted by improvised explosive devices (IEDs). Current and emerging US guidance directs that forces must be able to rapidly deploy, immediately employ upon arrival in the theater, and be continuously sustained throughout the operation. These forces can operate cohesively and maintain situational awareness even while separated by great distances. However, these operations outpace the ability of the logistics tail to keep up, so new methods of maneuver must be matched by new methods of agile sustainment. NATO commanders also require sustainment capabilities that can support forces that will be rapidly deployed, immediately employed upon arrival in theater, and conduct widely dispersed operations with lightning agility. JPADS delivers just such a capability (Benney, 2005).

The airdrop sequence for ballistic and guided airdrops is shown in Figure 1. This sequence is further broken down, and the terminology for CARP calculation variables is defined in Figure 2 from AFI 11-231, Computed Air Release Point Procedures.

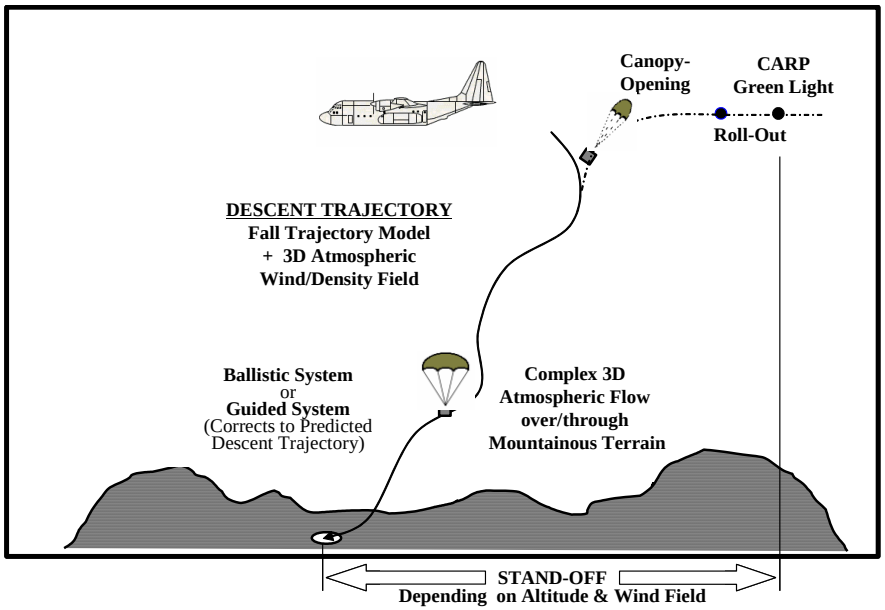

Figure 1. Depiction of Airdrop Sequence (Hattis, et al., 2006)

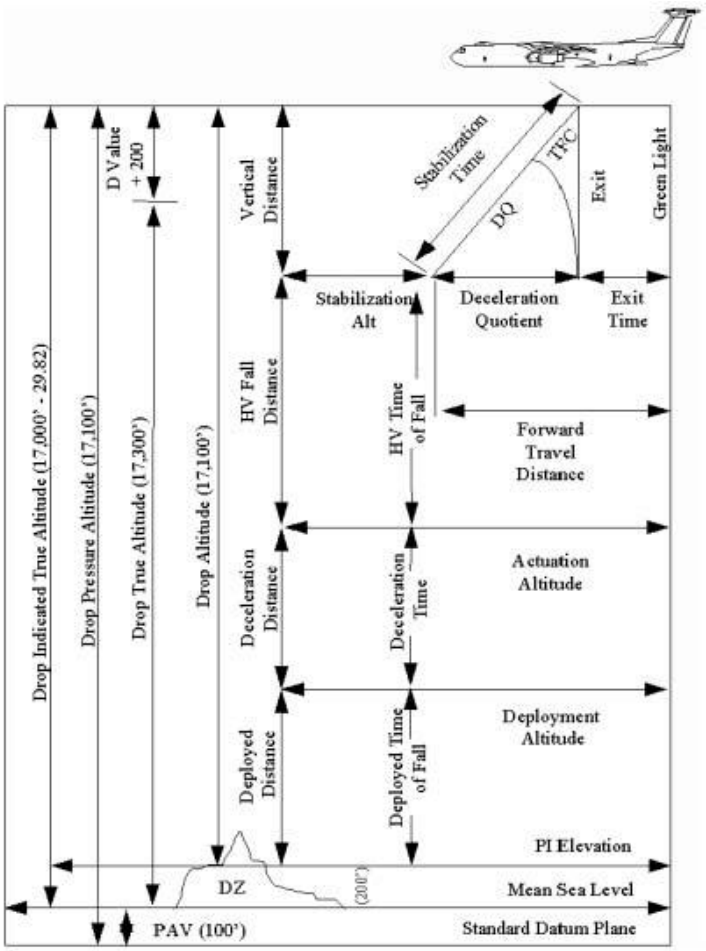

Figure 2. High Altitude Airdrop Terminology (AFI 11-231, 2005)

According to AFI 11-231, the minimum required wind data prior to a high altitude airdrop are a ballistic wind and a deployed wind. The ballistic wind is a vectorial average of the winds between the drop altitude and the actuation altitude (or ground level for single stage airdrops). A deployed wind is the vectorial average between the actuation altitude and the surface. These winds can be provided by a weather forecaster, but more commonly are computed by the aircrew from forecast winds at 1,000 foot intervals (AFI 11-231, 2005).

The JPADS-MP system operates in the cockpit on a high altitude compatible laptop computer that is connected to Combat Track II (CTII) secure satellite communication system (Benney, 2005). The roll-on/roll-off capability of the equipment, shown in Figure 3, does not require permanent modification of each aircraft, and allows multiple aircraft to share the limited number of JPADS hardware systems in operation. There is no direct interface to the aircraft systems, so once a revised CARP is calculated and displayed on the laptop, the aircrew manually enters it into the aircraft navigation system.

Figure 3. JPADS Components (QinetiQ- North America, 2008)

Current Sources of Winds for JPADS Operations

Michael Wuest of the U.S. Air Force Flight Test Center and Richard Benney of the Natick Soldier Center summarized the available wind sources and the benefits and shortcomings of each in a 2005 paper on precision airdrop. After payload release, winds affect the direction of travel and time of fall. The JPADS mission computer computes winds using data from the aircraft's airspeed, pressure, and temperature sensors, as well as navigation sensors. Wind data may also be entered manually using information relayed from the actual drop zone or from weather forecasts. Each type of data has benefits and drawbacks. Aircraft sensor winds are very accurate but may not reflect the weather conditions over the DZ because the aircraft is not able to fly from the ground to altitude over the DZ. Ground winds are typically much lighter than winds at altitude, particularly at high altitude. Forecast winds are predictions and do not reflect wind speeds and direction at the different altitudes. The increase in wind velocity with altitude is not usually linear. Therefore, if the correct wind profile is not determined and entered into the mission computer, the default assumption of a linear wind profile adds to errors in CARP computation (Wuest and Benney, 2005).

The resolution of wind forecasts that the Air Force Weather Agency (AFWA) currently provides to aircrew for JPADS operations is described by Capt David Gemas in his 2007 research on JPADS weather input. The forecasts are called 4-dimensional because they include x, y, and z spatial coordinates as well as a temporal coordinate. AFWA generates these forecasts in resolution of 5 km, 15 km, and 45 km. In 4-D forecast models, the resolution refers to how closely spaced the weather data points are

on the horizontal grid plane. Higher resolution means more data available, but also means a larger data file, with greater bandwidth and longer time required for transmission. The 5 and 15 km models are run every 12 hours and the 45 km model is run every 6 hours with each model run predicting 24 hours of weather (Gemas, 2007).

These winds are updated in flight through the release of a dropsonde near the drop zone just prior to the airdrop. The GPS dropsonde is a hand-launched probe that measures atmospheric data near the drop zone while falling at 70-90 feet per second. The dropsonde radio is programmed by the crew in 0.5 MHz increments between 400.5 and 405.5 MHz (HQ AMC JPADS CONEMP, 2009). It transmits its position during descent to an onboard dropsonde receiver connected the aircraft's lower UHF antenna. The dropsonde receiver then feeds the GPS position data to the MPS laptop to derive the wind profile. This initial wind profile is combined with the pre-flight forecast winds, and the resulting wind profile is used to generate either a release point for a ballistic payload, or in some instances, a Launch Acceptability Region (LAR) for guided payload delivery (AMC Single Pass Airdrop Workshop, 2009).

The GPS dropsonde is the most proven current source of wind updates for JPADS operations. Because variations in time and location of data collection can influence wind estimation, especially at lower altitudes, operators should consider the use of dropsondes to measure winds in the objective area as close to drop time as possible. The dropsonde does not need to be dropped by the aircraft performing the cargo airdrop, but could be deployed from another aircraft, or from a jet fighter, before the cargo plane arrives (Wuest and Benney, 2005).

Temperature Retrieval from Satellite Sounding and Wind Derivation

Molecular absorption by atmospheric gases provides an excellent tool for measuring temperatures from satellites. By knowing the concentration of a gas in the atmosphere and its mass absorption coefficient for a given wavelength, we can determine an optical depth. When a particular wavelength is measured from the atmosphere from above, the altitude that the radiation is coming from can be determined.

If the atmosphere strongly absorbs the wavelength being measured, any emissions from the surface or lower atmosphere will not make it to space. Instead, the strongest emissions received will be from an altitude corresponding with the peak in the weighting function for that wavelength. The usefulness of an individual measurement is limited, but when measurements are combined from a series of sensors, each receiving a slightly different wavelength near a strong molecular absorption line, a temperature profile can be constructed.

Since the gas will have a different optical depth for each wavelength, each sensor will "see" down to a different altitude in the atmosphere. A sensor at the center of an absorption line will measure the temperature near the top of the atmosphere, while farther from the absorption peak a sensor may receive surface temperature. Matching these individual measurements to a model of the atmosphere through an iterative process can yield a full temperature profile.

The most commonly used gases in temperature sounding are CO_2, water vapor, oxygen and ozone (CO_2 and oxygen having the advantage that they are well mixed throughout the atmosphere making their density easy to determine). For good results from ozone or water vapor sounding, local concentrations would need to be determined

through another process or model. Without knowing concentration, the altitude for water vapor returns is difficult to determine, but returns can still be useful for imagery. Common wavelengths used by geostationary satellites are in the vicinity of 15 microns (CO_2), 9.6 microns (ozone), and 5-8 microns (water vapor).

The determination of temperature by passive atmospheric sounding relies on Schwarzchild's equation. Vertical sounding theory begins with the integrated form of this equation:

$$L_\lambda = L_0\, e^{-\frac{\delta_0}{\mu}} + \int_0^{\delta_0} e^{-\frac{\delta_0-\delta_\lambda}{\mu}}\, B_\lambda(T)\frac{d\delta_\lambda}{\mu} \qquad (1)$$

From the optical depth δ, height in the atmosphere can be determined. Schwarzchild's equation is manipulated to yield a weighting function for an individual wavelength. The peak in this weighting function is used to assign an altitude to the measured radiance (Kidder and Vonder Haar, 1995)

$$W_\lambda(h,\mu) = \frac{d}{dh}\left(\tau_\lambda{}^{1/\mu}\right) \qquad (2)$$

The problem of retrieving temperature from brightness temperature measurements is complicated. A series of observed radiances is measured and matched with the corresponding weighting function for the wavelength of the measurement channel. The process for solving the inverse problem, determining what temperature and trace gas concentration profiles could have produced that set of observed radiances, is laid out by Stanley Kidder and Thomas Vonder Haar in their text *Satellite Meteorology*. Because the forward problem of determining the radiance from a known temperature and trace gas concentration profile is easy, the scheme to solve the inverse problem is to make a series

of profile guesses until convergence is achieved. Kidder and Vonder Haar's iterative process is:

1. A first-guess temperature profile is chosen
2. The weighting functions are calculated
3. The forward problem is solved to yield estimates of the radiance in each channel of the radiometer.
4. If the computed radiances match the observed radiances within the noise level of the radiometer, the current profile is accepted as the solution.
5. If convergence has not been achieved, the current profile is adjusted.
6. Steps 3 through 5 (or 2 through 5) are repeated until a solution is found. (Kidder and Vonder Haar, 1995)

Polar orbits are much lower than geostationary orbits, and do not need short wavelengths to have useful resolution. For this reason, these satellites can take advantage of microwave absorption features like oxygen's strong line at 60 GHz (5 mm). The Advanced Microwave Sounding Unit is a polar orbiting satellite that uses 11 channels on the edge of this oxygen line.

The weighting functions for these channels plotted against pressure in millibars (mb), as depicted in Grant Petty's text *A First Course in Atmospheric Radiation* is shown in Figure 4. For each wavelength, approximate altitude can be determined using the pressure for the point where the corresponding channel's weighting function reaches a maximum.

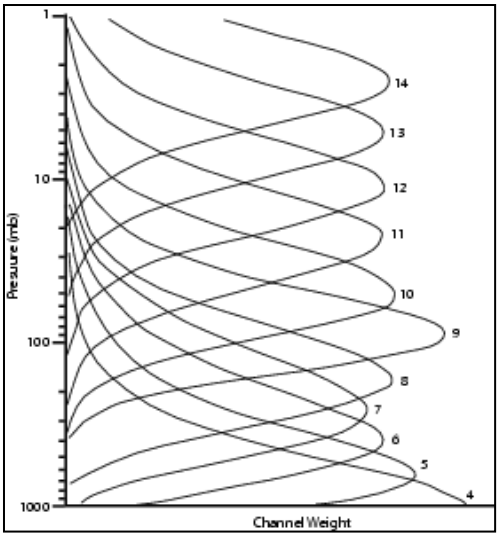

Figure 4. Microwave Weighting Functions for AMSU Sounding Channels (Petty, 2006)

For the high resolution Atmospheric Infrared Sounder (AIRS) some of the weighting functions are shown in Figures 5a and 5b. These plots illustrate that each of these weighting functions (corresponding to 40 channels in the vicinity of the 4.3 μm CO_2 absorption line) reaches a maximum at a slightly different pressure level.

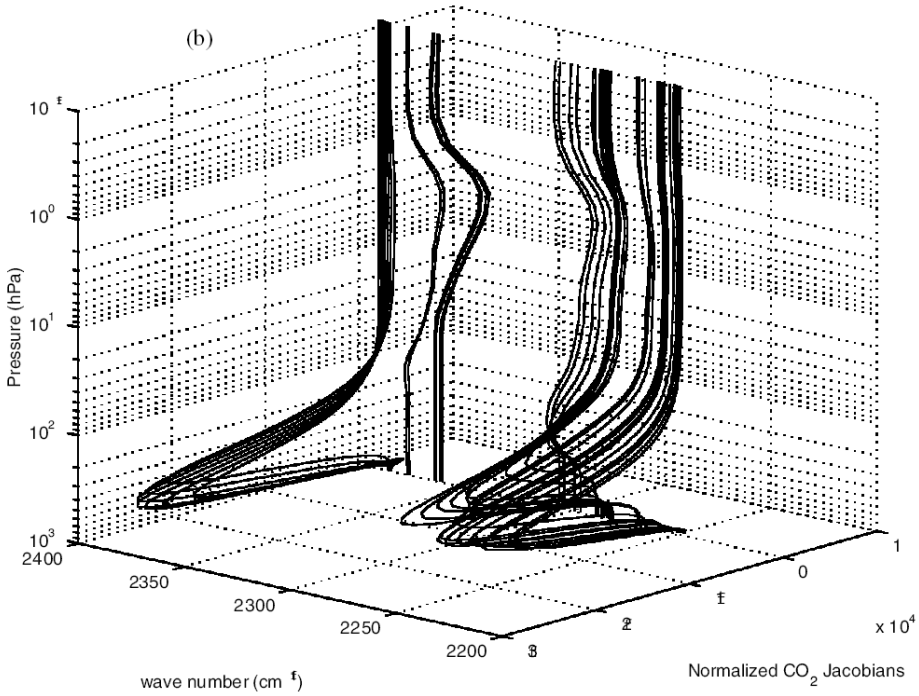

Figure 5a. Example Weighting Functions for AIRS Sounding Channels (Crevoisier, et al., 2003)

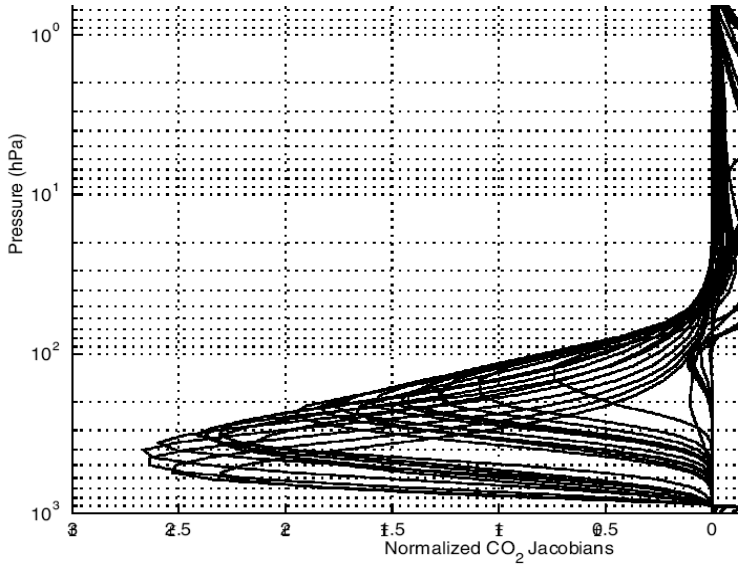

Figure 5b. Weighting Functions for AIRS Sounding Channels near 4.3 µm (Crevoisier, et al., 2003)

GOES and AMSU Programs

The Geostationary Operational Environmental Satellite (GOES) program includes a series of 14 weather satellites placed in geosynchronous orbit since 1974. GOES 10, 11, and 12 are currently in operation and are transmitting data and imagery. The component that is critical to this research is the GOES Sounder. The sounders are filter wheel radiometers containing 18 thermal infrared channels plus a visible channel with 10-km linear resolution (Ma, et al., 1999). A NOAA graphic depicting the components of the GOES Sounder is shown in Figure 6.

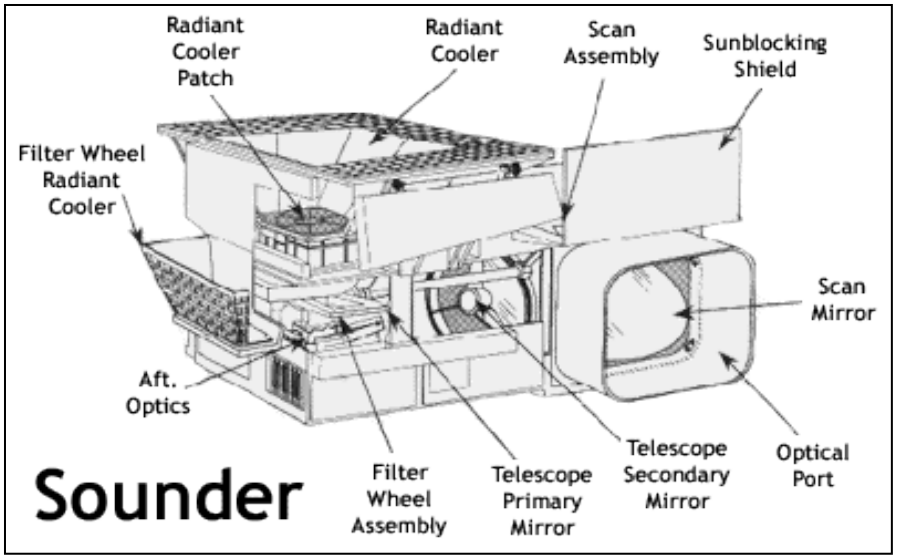

Figure 6. NOAA GOES Sounder Components

The thermal infrared channels provide measurements of radiance from the earth's surface, clouds, and atmospheric carbon dioxide (CO_2), moisture (H_2O), and ozone (O_3). The GOES sounder channels were selected to permit atmospheric temperature and moisture profile retrieval with high spatial (10 km at nadir) and temporal (hourly) resolution. (Ma, et al., 1999). This CIMSS graphic (Figure 7) shows the various channels used for sounding by the GOES satellites:

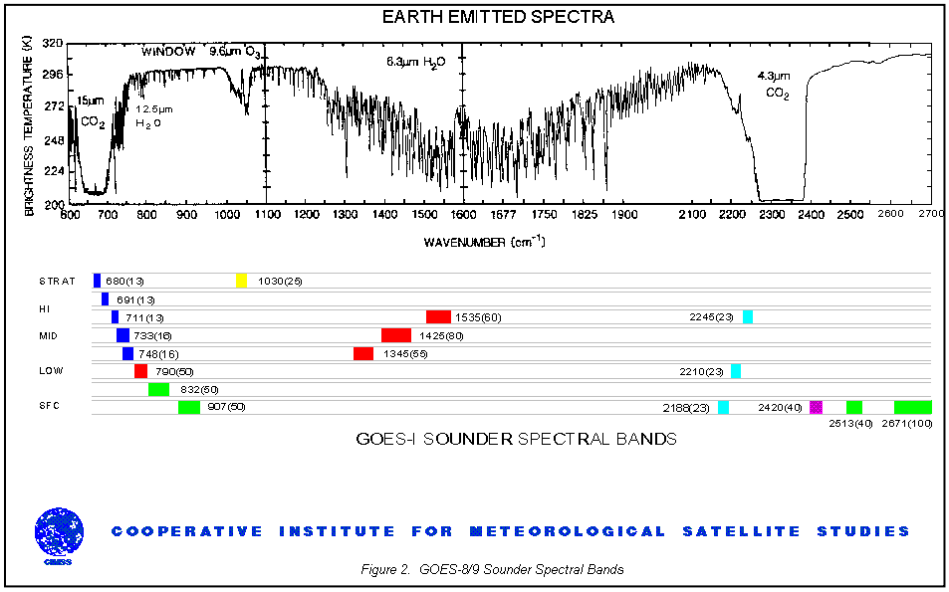

Figure 7. Emission Spectra and GOES Spectral Bands

The GOES window bands are located in spectral regions where the atmosphere is relatively transparent and are selected so that the atmosphere becomes progressively more opaque from one spectral band to the next. As the atmosphere becomes more opaque, the sensed signal comes from higher up in the atmosphere (Menzel, et al., 1998). The process of retrieving GOES profiles is shown in Figure 8.

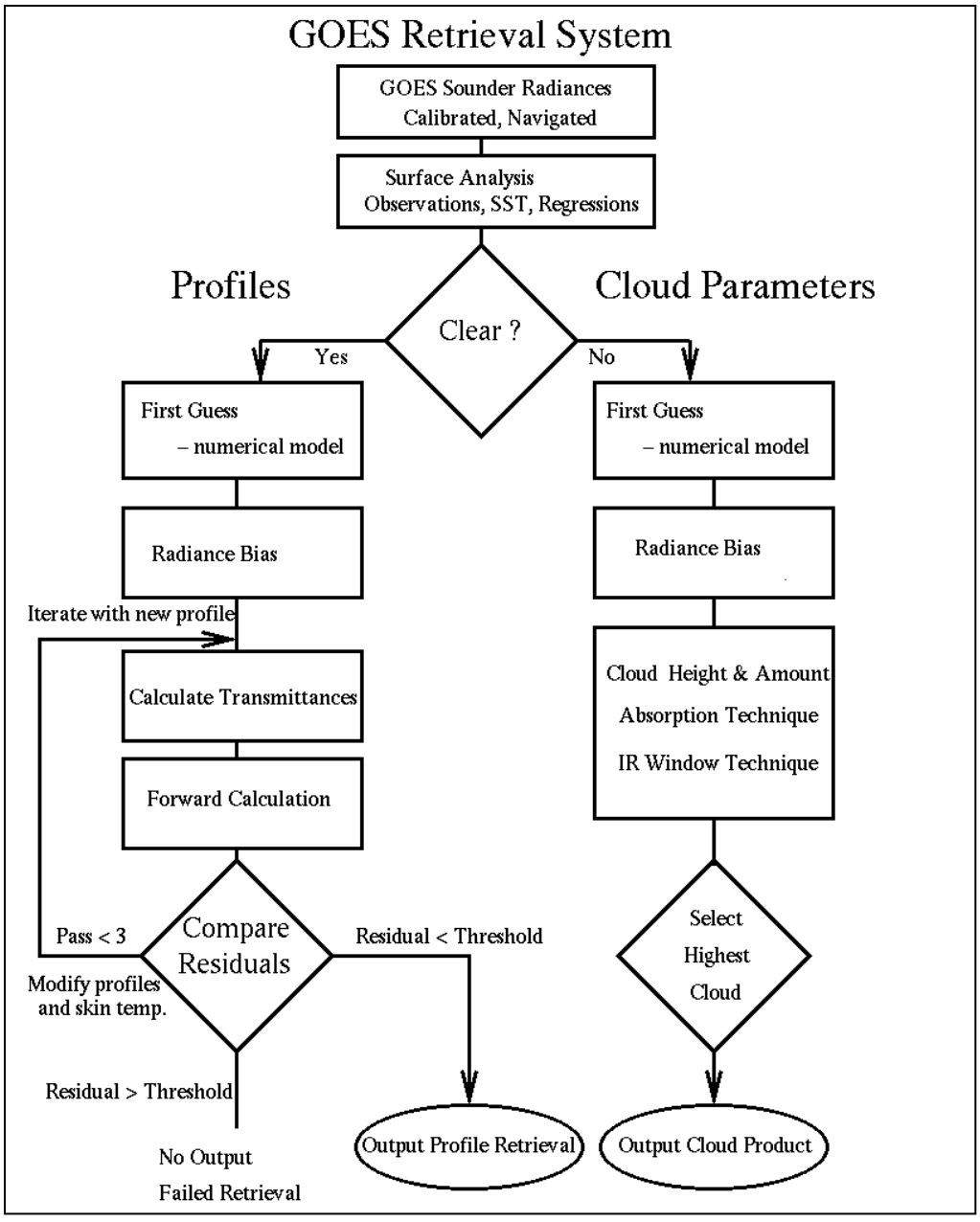

Figure 8. Flowchart of GOES Sounder Data Processing (Menzel, et al., 1998)

In a paper detailing the application of GOES soundings to weather forecasting, W. Paul Menzel et al. describe the progress made in computing thermal winds. In mid latitudes, using the assumption of a balanced atmosphere, thermal wind profiles have been used successfully to estimate atmospheric motions in clear sky situations. The thermal wind profiles are derived from a field of soundings, using horizontal temperature gradients to infer vertical motion gradients. Modelers often prefer this form of the sounding product over the geopotential height fields. In combination with features tracked in sequences of sounder water vapor images, these sounder thermal winds have proven to be valuable in depicting near mid-tropospheric motions. Such information, especially in the northwest sector of the near hurricane environment, has proven to be very useful. Improvements in the total suite of GOES wind field estimations have reduced the average 72 hour forecast error for a given storm feature of 360 nautical miles (670 km) by about 20% in a variety of research and operational models (Menzel et al., 1998).

UW-CIMSS Satellite-Derived Wind Algorithm

The University of Wisconsin's Cooperative Institute for Meteorological Satellite Studies has done extensive research into wind determination from satellite observations. Early successes came from automating the process of deriving wind direction and velocity by observing cloud movement in subsequent frames of visible and IR satellite images. An alternate method, which does not rely on cloud presence at each altitude for which wind is derived is their CO_2-Infrared Window Ratio Method, or the CO_2 Slicing method. Due to the fact that the emissivities of ice clouds and the cloud fractions for the Infrared Window and CO_2 Channels are roughly the same, this method is effective where

semi-transparent clouds are present. The user's guide for their algorithm describes this equation for height assignment for each measurement (Olander, 2001):

$$\frac{R(CO_2) - R_{cl}(CO_2)}{R(IRW) - R_{cl}(IRW)} = \frac{nE(CO_2)\,[R_{cbd}(CO_2,P_c) - R_{cl}(CO_2)]}{nE(IRW)\,[R(IRW,P_c) - R_{cl}(IRW)]} \quad (3)$$

where *n* is the fraction of field of view covered by cloud and *E* is the cloud emissivity. The ratio of the measured radiance difference between cloudy and clear sky for the CO_2 and Infrared Window (IRW) channels is calculated. This ratio is compared to a series of possible solutions computed at incremental pressure values. The pressure value that produces a result most closely matching the ratio value on the left side is used as the pressure of the cloud. The radiance values on the right−hand side of the equation require a first guess (model forecast) field, as with the H_2O−Infrared Window Intercept method, in order to properly estimate the atmospheric profile at the target location.

Typically, for geostationary satellite soundings, the 11 μm infrared window channel and the 13 μm CO_2 channel are used with this method. Any two channels, however, can be used provided their weighting functions (molecular absorption characteristics) are sufficiently dissimilar while the effective cloud amount is the same for both channels. This method can fail when the observed and clear radiance difference falls below the instrument noise for either channel, such as low broken cloud or very thin cirrus scenes (Olander, 2001).

Geostrophic Wind

Once atmospheric temperature profiles are determined, they can be used to derive the wind direction and velocity. From the temperature soundings, the thickness of each pressure layer can be estimated. If the height of one of these pressure levels is known

from either a surface or upper atmosphere observation or forecast, the heights of all other pressure levels can be calculated. By combining heights from a series of sounding locations, isobaric pressure surfaces can be constructed, and from these pressure surfaces, several relationships can be used to determine winds. One of these is the geostrophic wind, which is related to the gradient of the geopotential heights:

$$V_g = \frac{1}{f}\,\hat{k} \times \nabla\Phi \tag{4}$$

where Φ is the geopotential (gz), f is the Coriolis parameter, and $\hat{k}$ is a vertical unit vector (Kidder and Vonder Haar, 1995). Figure 9 graphically depicts the relationship between the geostrophic wind V_g and the pressure gradient force, P and the Coriolis force, C.

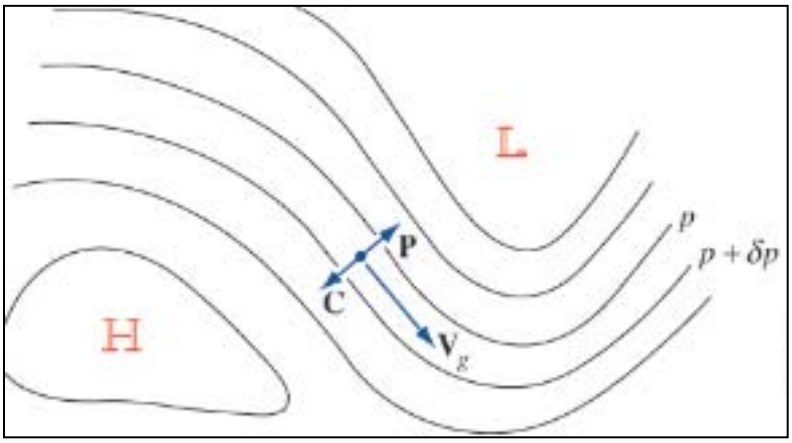

Figure 9. Depiction of Geostrophic Wind Relationship (Wallace and Hobbs, 2006)

$$u_g = -\frac{1}{f}\frac{\partial\Phi}{\partial y} \tag{5}$$

$$v_g = \frac{1}{f}\frac{\partial\Phi}{\partial x} \tag{6}$$

In component form the term u is used for the wind vector from the west, and v is the wind from the south. In equations 5 and 6, u_g and v_g are the components of the

geostrophic wind. Another relationship determines the magnitude of the gradient wind by:

$$V_{gr} = \frac{2\,V_g}{1+(1+4\frac{V_g}{f\,R_T})^{1/2}} \quad (7)$$

where R_T is the radius of curvature of the trajectory of an air parcel. Comparisons made in 1982 showed the gradient wind to most closely match rawinsonde data. The agreement for winds aloft (compared at 300 hPa) was good with a correlation coefficient of 0.87, but for lower altitude 850 hPa winds, the accuracy was much lower. For one of the days of the experiment, satellite-derived and rawinsonde measured 850 hPa winds were essentially uncorrelated (Kidder and Vonder Haar, 1995).

Thermal Wind

The thermal wind equation defines the vertical shear in geostrophic wind as a function of the temperature gradients. The horizontal temperature gradient determines the change in thickness of a layer of the atmosphere, as shown in Figure 10. This change in thickness will cause there to be a different slope on the top surface of the pressure layer than on the bottom surface. The thermal wind is not a wind at all, but a measurement of the wind shear between two levels. The thermal wind relationship does not actually predict the magnitude and direction of the geostrophic wind, it determines the difference in wind vectors between the top surface and the bottom surface of the layer.

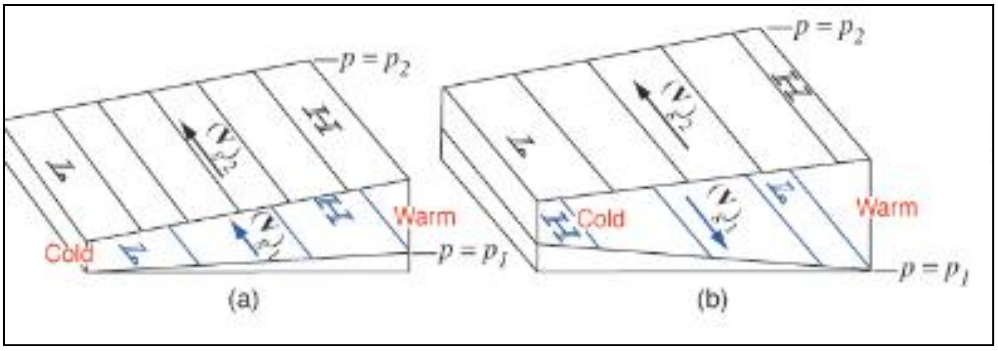

Figure 10. Thermal Wind Relationship (Wallace and Hobbs, 2006)

In component form, the thermal wind equations are described by Wallace and Hobbs as:

$$(u_g)_2 - (u_g)_1 = -\frac{g_0}{f}\frac{\partial(Z_1 - Z_2)}{\partial y} \tag{8}$$

$$(v_g)_2 - (v_g)_1 = \frac{g_0}{f}\frac{\partial(Z_1 - Z_2)}{\partial x} \tag{9}$$

Accuracy of Satellite-Derived Winds

The potential accuracy of satellite-derived winds has been well established. Figure 11 shows the multiplatform satellite analysis (red) and that obtained primarily from aircraft data (blue) for Hurricane Michelle from the 2001 hurricane season. The winds are along a north-south line through 84.1 degrees W. The results show that the two methods compare reasonably well (CIRA Annual Report, 2005).

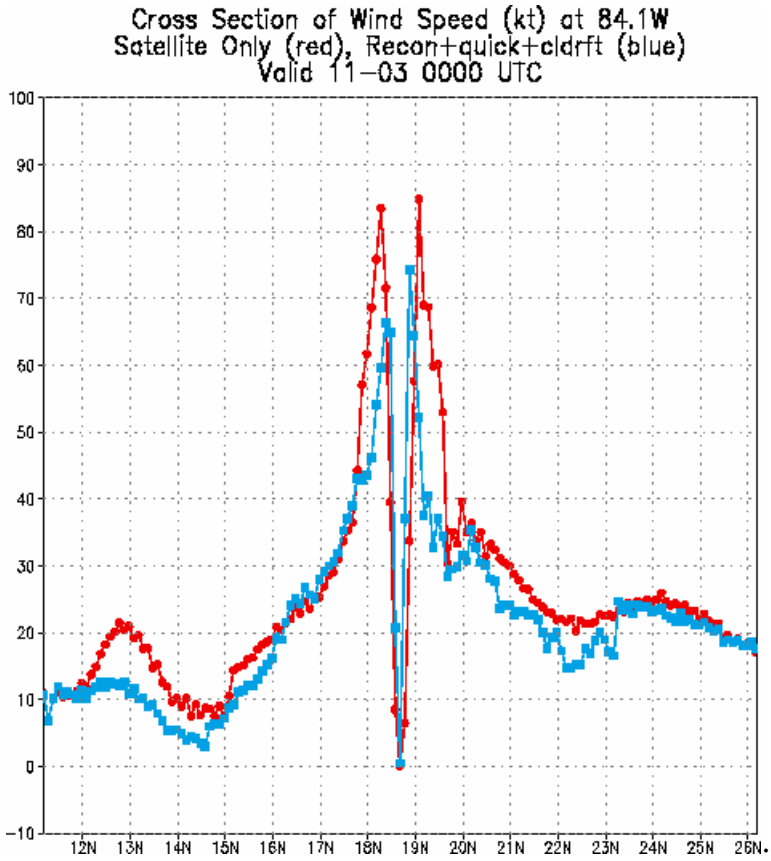

Figure 11. Comparison of Satellite-Derived (red) and Aircraft Measured (blue) Wind Strengths from Hurricane Michelle in 2001 (CIRA Annual Report, FY 04/05)

METEOSAT and METOP Satellite Systems

The European Organisation for the Exploitation of Meteorological Satellites (EUMETSAT) operates two generations of geostationary METEOSAT satellites and a polar orbiting MetOp satellite. The MetOp-A satellite is equipped with the Infrared Atmospheric Sounding Interferometer (IASI). This instrument improves accuracy and resolution of atmospheric temperature and humidity soundings. The IASI is a Fourier Transform Spectrometer based on a Michelson Interferometer coupled to an integrated imaging system that observes and measures infrared radiation emitted from the Earth in the band between wavelengths of 3.4 and 15.5 microns. This enables the instrument to establish temperature profiles in the troposphere and the lower stratosphere. The IASI

instrument delivers temperature profiles with an accuracy of 1 Kelvin and a vertical resolution of 1 kilometer. With a 2000 kilometer swath width on the Earth's surface, global coverage is achieved in 12 hours. To optimize coverage, the IASI measurement cycle is synchronized with that of the AMSU instruments (European Space Agency, 2006). A depiction of a vertical temperature profile obtained by IASI sounding is presented in Figure 12.

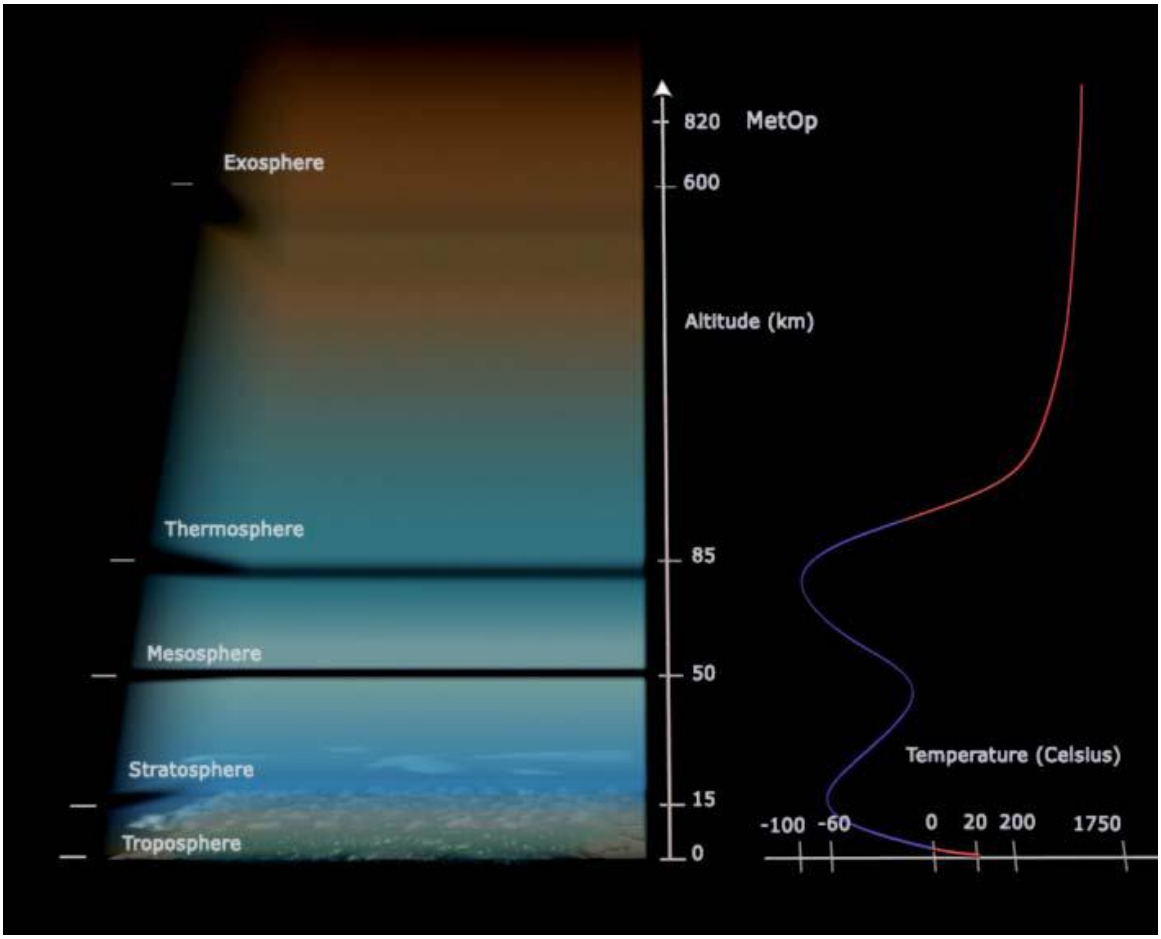

Figure 12. IASI Derived Temperature Profile (ESA, 2006)

There are multiple satellite data sources and derivation techniques in use to derive altitude wind direction and magnitude. This research will focus on brightness temperature sounding data, and an algorithm to derive winds from the calculated

temperature and pressure gradients. A significant advantage of this method is that the results do not require the presence of clouds as needed for the feature tracking wind determination methods. A limitation is the inability to derive winds below heavy cloud cover. The best, and most operationally useful, solution would be to combine the IR sounding technique investigated in this research, with wind data derived from microwave soundings and cloud feature tracking. This would increase the availability of wind profiles in areas with cloud cover.

Atmospheric Infrared Sounder (AIRS)

According to BAE Systems, NASA's Aqua spacecraft is collecting data on earth systems and weather features in a scope and detail not seen before. Aqua, launched on May 4, 2002, as part of the Earth Observing System, collects data related to global water cycles with the goal of improving weather prediction and scientists' understanding of climate change.

Hyperspectral sensing from space is a technique that delivers weather-balloon-quality measurements on a global scale. Using infrared hyperspectral sensing, AIRS passively measures temperature and humidity. The infrared region consists of a range of wavelengths that correlate with altitude. Measuring the brightness of infrared wavelengths that correspond to temperature, AIRS creates full and accurate mapping of temperature from the surface to more than 30 km in altitude.

Other AIRS features include twelve individually optimized arrays, each consisting of 4,500 detectors, which provide the system's high wavelength selectivity and initial signal processing. For high sensitivity operation, the detectors are cooled to 58 Kelvin by a first-of-its-kind, space-qualified Stirling pulse tube cryocooler (BAE, 2010). A

schematic diagram of the AIRS instrument configuration is presented in Figure 13. Figure 14 describes the sounder's scan geometry and field of view.

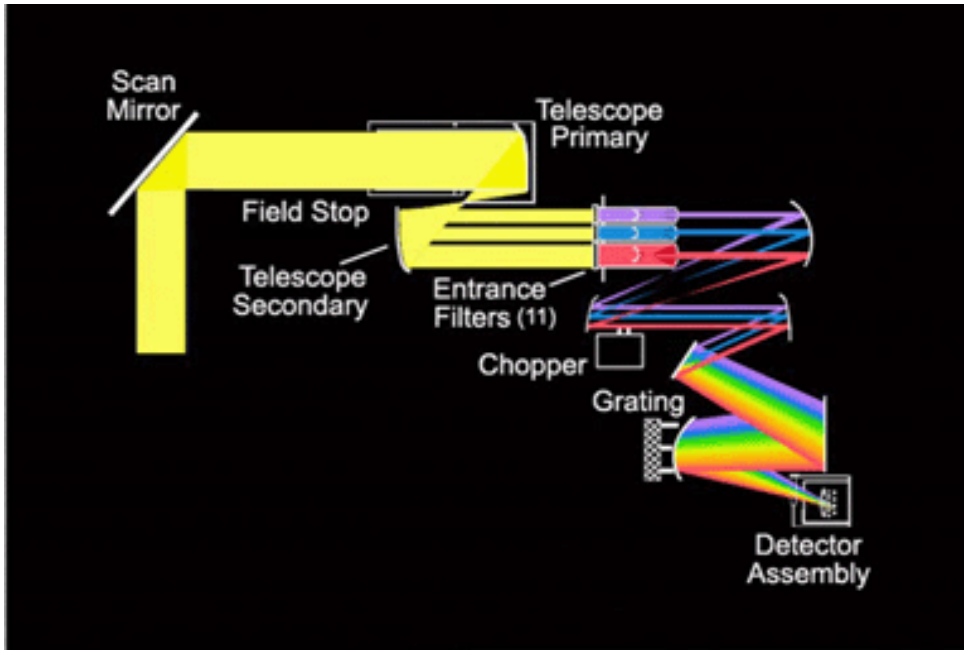

Figure 13. AIRS Instrument Layout (JPL AIRS Animation)

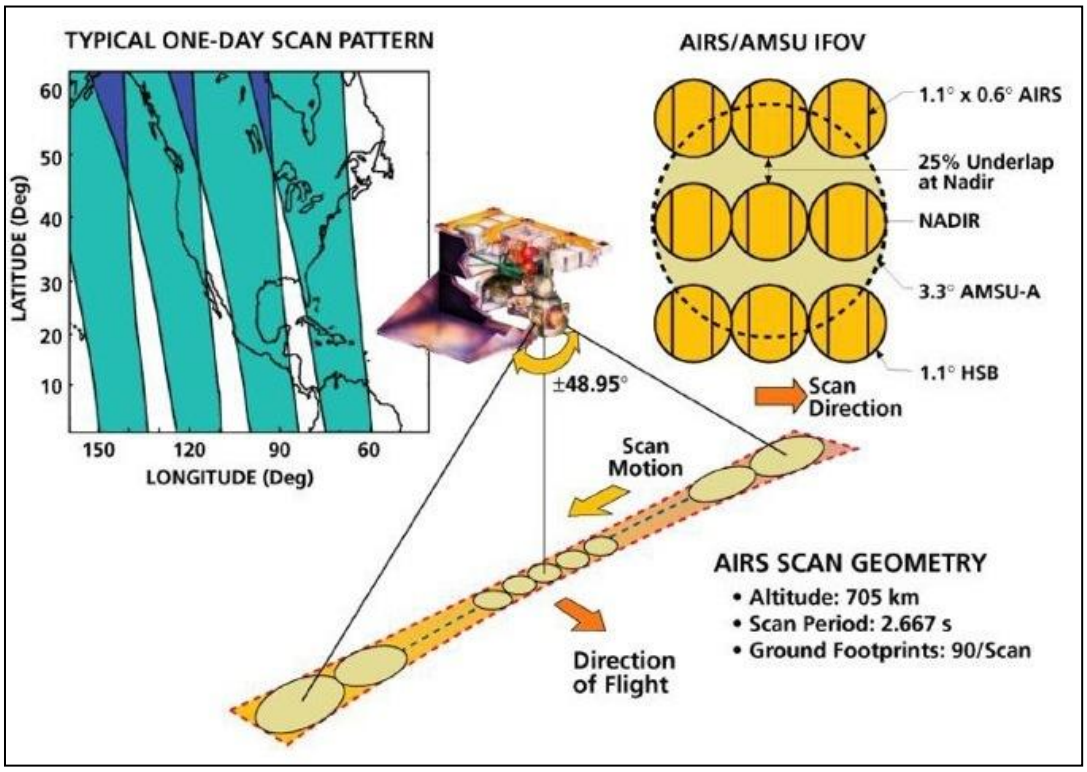

Figure 14. Scan Geometry for AIRS Instrument (JPL-How AIRS Works)

Global Forecast System (GFS)

The GFS is run four times per day (00 UTC, 06 UTC, 12 UTC, and 18 UTC) out to 384 hours. The initial forecast resolution was changed on May 31, 2005 to T382 (equivalent to about 40-km grid-point resolution) with 64 levels out to 7.5 days (180 hours). At later forecast times, the GFS has a resolution of T190 (equivalent to about 80-km resolution) and 64 levels between 24 and 384 hours. All GFS runs get their initial conditions from the Gridpoint Statistical Interpolation (GSI) global data assimilation system (GDAS) as of 1 May 2007, which is updated continuously throughout the day (MetEd, 2007).

Radiosonde Sounding System

A global network of sites release weather balloons with attached rawinsondes, or radiosondes daily, usually 00Z and 12Z. The accuracy of the atmospheric measurements made by these radiosondes has been well established, so radiosonde data provides temperature and wind profiles for validation of satellite-derived data. The Meteorological Resource Center's website, WebMET.com, describes the radiosonde technology and process: Radiosonde sounding systems use sensors carried aloft by a small, balloon-borne instrument package (the radiosonde, or simply "sonde") to measure vertical profiles of atmospheric pressure, temperature, and moisture (relative humidity or wet bulb temperature) as the balloon ascends. In the United States, helium is typically used to inflate weather balloons, but some locations use hydrogen. The altitude of the balloon is typically determined using thermodynamic variables or by satellite-based Global Positioning Systems (GPS). Pressure is measured by a capacitance aneroid

barometer or similar sensor. Temperature is typically measured by a small rod or bead thermistor. Most commercial radiosonde sounding systems use a carbon hygristor or a capacitance sensor to measure relative humidity directly, although a wet-bulb sensor is used by some systems.

A radiosonde includes electronic subsystems that sample each sensor at regular intervals (usually every 2 to 5 seconds), and transmit the data to a ground-based receiver and data acquisition system. Most commercial radiosonde systems operate at either 404 MHZ or 1680 MHZ. Once the data are received at the ground station, they are converted to engineering units based on calibrations supplied by the manufacturer. The data acquisition system reduces the data in near-real time, calculates the altitude of the balloon, and computes wind speed and direction aloft based on information obtained by the data systems on the position of the balloon as it is borne along by the wind. The radiosondes are typically smaller than a shoebox and weigh only a few hundred grams.

Upper-air winds (horizontal wind speed and direction) are determined during radiosonde ascents by measuring the position of the radiosonde relative to the earth's surface as the balloon ascends. By measuring the position of the balloon with respect to time and altitude, wind vectors can be calculated that represent the layer-averaged horizontal wind speed and wind direction for each successive layer. The position of the radiosonde was originally tracked using radio direction finding techniques (RDF) or by radio navigation network, but the use of satellite-based GPS has become more common (WebMET.com, 2002).

III. Methodology

The purpose of this chapter is to describe the sources of data used in this research, and the process developed to filter and manipulate this data into a useful format. The project relies on several data sources to develop final wind profiles. For this research, a notional dropzone location is selected so that the time of satellite overpass closely coincides with a scheduled rawinsonde measurement. The three part process begins with an initial field of forecast temperature, wind speed, and wind direction values in a region surrounding the objective area. The second source of data, and the focus of this research, is a three dimensional field of satellite measured temperature values covering the same area as the forecast data. The final step in this project is to use the measured satellite temperatures to validate and/or update the forecast to create a more accurate vertical wind profile over the selected drop zone coordinates. A flowchart depicting the sources of data used and the order of these steps is shown in Figure 15.

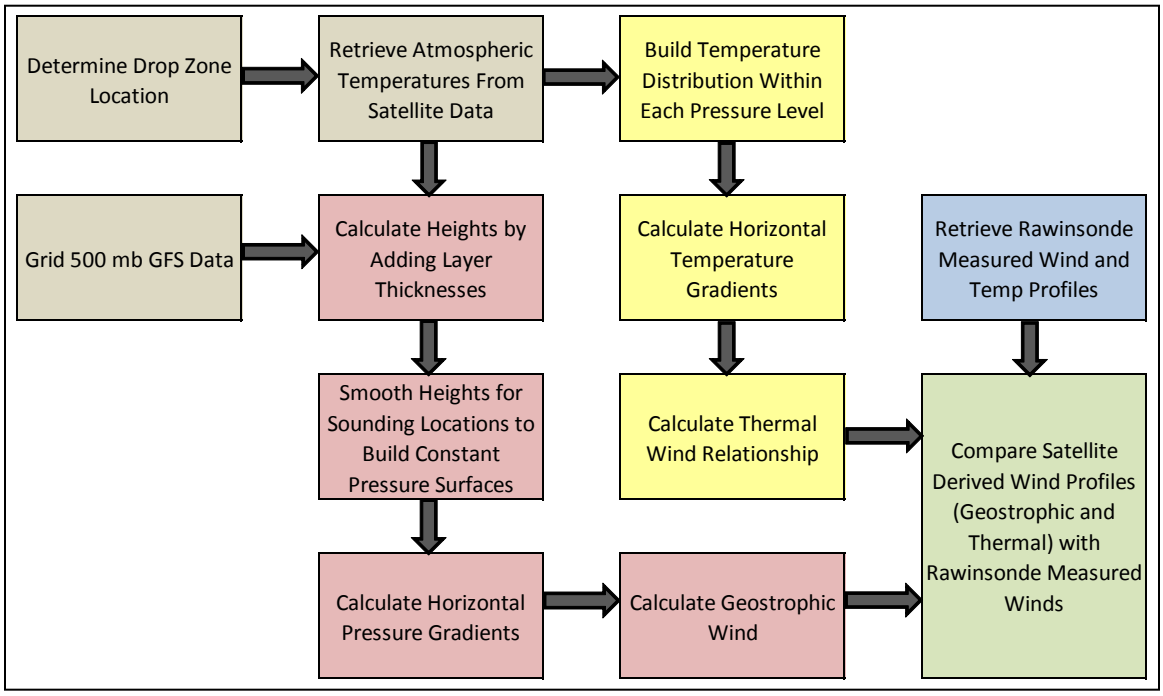

Figure 15. Flowchart of Data Sources and Wind Derivation Sequence

Data Sources

The two sources of gridded forecast data evaluated are 6 hour Global Forecast System (GFS) data and a 4 dimensional weather product specifically generated by the Air Force Weather Agency (AFWA) for use in JPADS operations. Both of these products provide the needed temperature and wind values, with the most significant differences being the resolution of the available data. These differences are shown in Table 3.1: (MetEd, 2007 and Air Force Weather Agency)

Table 3.1 Comparison of Resolutions for GFS and AFWA JPADS 4-D Forecasts

	Horizontal	**Vertical**	**Temporal**
Global Forecast System (GFS)	0.9°/40 km	64 Layers	6 Hours
AFWA JPADS 4-D Forecast	5 km (in contingency windows)	56 Layers	3 Hours

Figure 16 represents how a region covered by the AFWA high resolution, contingency window is nested within a lower resolution weather model window. The 15 km model is run over a large region surrounding the contingency window, and is used to establish boundary conditions for the nested mode. Then, the higher resolution 5 km model, using the 15 km model output as initial conditions, is run for the smaller window. The better resolution should more accurately account for effects caused by terrain features and small-scale motion in the atmosphere, leading to a better wind forecast for the objective area at the time of the airdrop.

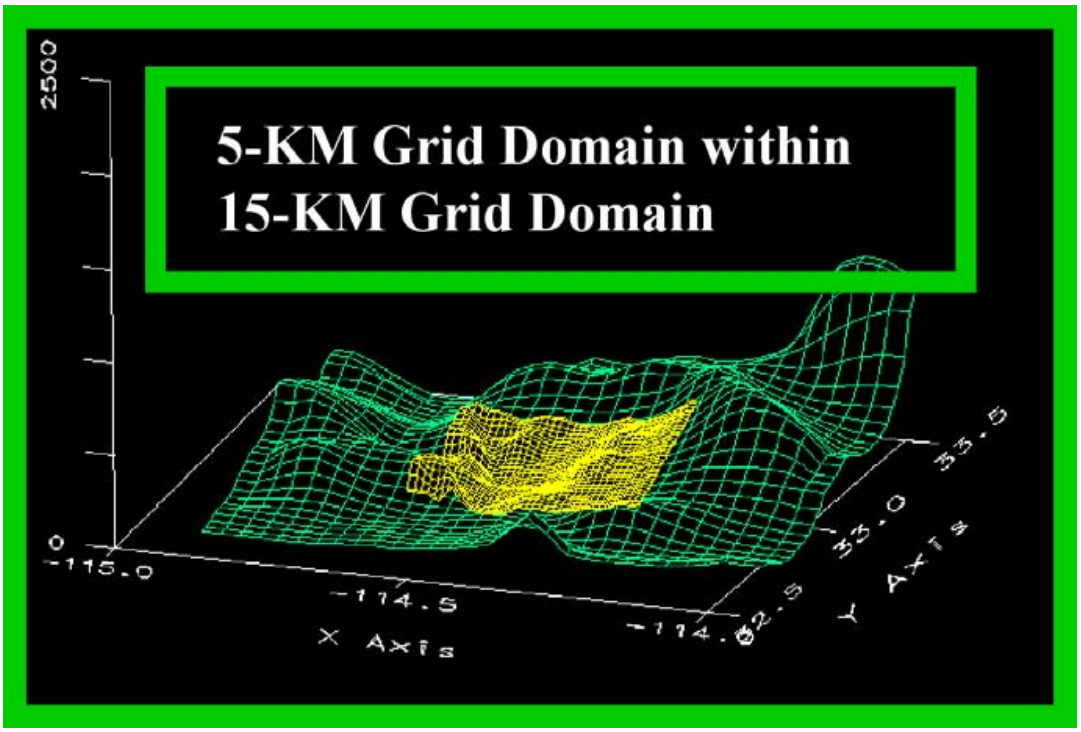

Figure 16. Nested Contingency Window Illustration (QinetiQ-North America, 2008)

Gridded forecast weather data from AFWA's JPADS 4-D product can be used both to set boundary conditions and to fill in the objective area initial values. Another option would be to select several 1-D, vertical weather profiles, also available from AFWA. By selecting profiles for multiple grid points surrounding the drop zone location, the three-dimension initial value grid can be built. An example of one of these 1-D forecasts is shown in Figure 17.

A. Forecast Time, Drop Zone Location, Elevation

Valid Time: 1800Z 25 NOV 2009 Data Source: WRF

Forecast Model Grid Pt: Latitude-> 31.99N Longitude-> 98.02W

Forecast Model Grid Pt Elevation: 1144 feet above MSL

Point of Impact: Latitude-> 32.00N Longitude-> 98.00W

Forecast Model Grid Point Bearing/Range from Point of Impact: 252DEG/1.67KM

(*Note! Model Grid Pt is nearest to entered Lat/Lon and is in decimal degrees format.)

B. Winds, Temperature, Pressure Altitude, D-Values, Ballistic Winds -

HEIGHT (KFT AGL)	(PRESS) (MB)	DIR (DEG)	SPEED (KNOTS)	TEMP (DEG C)	PRESS ALT (KFT MSL)	D-VALUE (FT)	BALLISTIC WINDS (DEG)	(KNOTS)
SFC	(983)	331	7	11	0.80	+0312	331	7
1	(948)	330	12	8	1.84	+0302	330	9
2	(913)	334	15	8	2.85	+0295	332	11
3	(880)	340	13	7	3.85	+0293	334	12
4	(848)	337	11	6	4.85	+0293	335	11
5	(817)	317	10	5	5.85	+0297	332	11
6	(787)	293	12	4	6.84	+0302	326	11
7	(758)	279	15	4	7.83	+0318	319	11
8	(730)	269	15	3	8.81	+0337	312	11
9	(703)	255	15	2	9.78	+0361	306	11
10	(677)	245	15	1	10.76	+0383	299	10
11	(651)	243	15	-1	11.73	+0416	293	10
12	(627)	246	15	-3	12.70	+0445	289	10
13	(603)	250	14	-5	13.67	+0472	285	10
14	(580)	255	14	-8	14.65	+0492	283	11
15	(558)	260	14	-10	15.62	+0520	281	11

Figure 17. AFWA 1-D JPADS Vertical Forecast Profile Format

Satellite Data

The first decision made in the selection of the most appropriate source of satellite data is whether to use data from geostationary or polar orbiting satellites. The primary advantage of a geostationary platform is that it is continually present over its assigned area. This leads to the availability of more frequent sounding data (usually hourly), and

makes feature tracking wind calculation possible. In addition to deriving wind direction from brightness temperature data, wind speed and direction can be calculated by automated algorithms which track the position of visible or IR cloud features in subsequent satellite images. Once an altitude is assigned to these features, additional wind speed and direction data is available to augment brightness temperature wind data.

The limitations of geostationary satellite sounding data are primarily caused by the sounder resolution. Due to the high orbital altitude of 35,800 km, the horizontal resolution of an instrument on a geostationary satellite is more than 40 times larger than it would be for the same instrument mounted on a satellite in a low altitude (700-1000 km) polar orbit. Vertical resolution, or the number of altitude layers that can be accurately resolved, is a function of the number of sounder channels measured. Current geostationary satellites only measure brightness on 15-20 channels.

Instruments in use on polar orbiting satellites are able to measure brightness temperatures on many more spectral channels. The Atmospheric Infrared Sounder (AIRS) on the Aqua satellite uses 2378 channels and the Infrared Atmospheric Sounding Interferometer on the European MetOp satellite uses 8461 channels. A weighting function is calculated for each of these channels, and the density of the data allows for the determination of atmospheric temperature at each of 100 or more layers to an accuracy of 1.0 ºC. The quality of data from this latest generation of infrared sounders is "expected to exceed temperature and humidity measurements of operational radiosondes". (EUMETSAT, 2007)

For this research, AIRS data from the polar orbiting Aqua satellite was used to determine the applicability of the technique. During each 90 to 100 minute orbit of the

satellite, the Earth rotates about 25 degrees, so each day, most locations on earth are covered by both an ascending and descending satellite pass. Near the equator, the coverage is not complete and the surface area missed is filled in by the next day's flight path. At latitudes greater than about 30 degrees however, each swath overlaps the previous one causing some locations to be sounded 4 times per day. Figure 18 illustrates this pattern by depicting three subsequent polar orbit tracks. Figure 19 expands the point by showing overlapping swath with for subsequent paths.

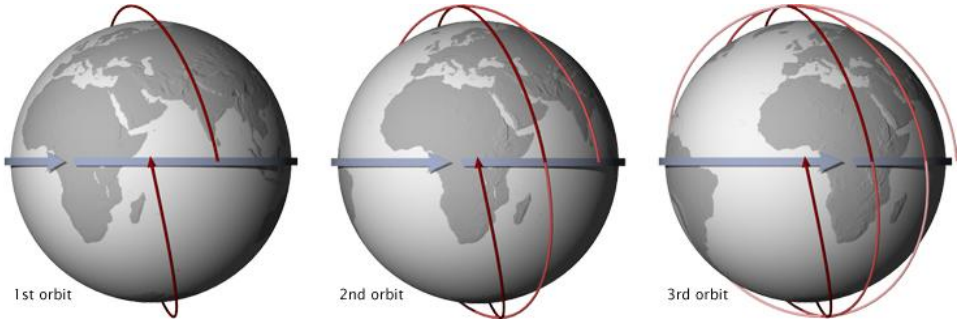

Figure 18. NASA Graphic - Sequential Polar Orbit Passes (NASA-Earth Observatory)

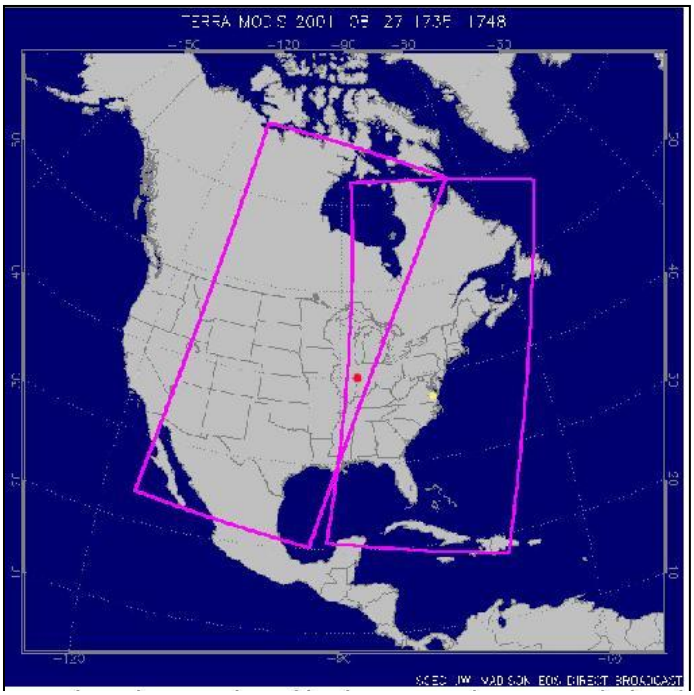

Figure 19. NASA Depiction of Overlapping Swath Width for Consecutive Descending Polar Orbit Passes for the Terra Satellite (NASA-Earth Observatory)

Once proven for AIRS data, the same technique could be used with data from other polar orbiting satellites with similar infrared sounders, NOAA 18, NOAA 10, MetOp A, and DMSP F16. Using all five platforms would reduce the mean time between overflight for a mid-latitude drop zone to 2.4 hours. For this source of wind data to be operationally valuable, it would need to be available close to the time of a planned airdrop. With multiple polar orbiting sounders to choose from, there would be many opportunities each day to schedule a JPADS airdrop for which sounder data (from one of these multiple platforms) is available from a satellite pass 1-2 hours prior to the drop.

Data Filtering and Processing

AIRS and AMSU sounder data files are available over the internet from the Jet Propulsion Laboratory (JPL). Individual data files cover six minutes of flight time, during which the platform travels approximately 1500 km and the AIRS-suite scan covers a swath roughly 1500 km wide. Level 2 data has been geolocated and processed to calibrate and correct brightness temperatures for sun position and instrument errors. The file format, Hierarchical Data Format-Earth Observing System (HDF-EOS), is a specialized form of HDF selected by NASA to standardize the format of the terabyte of data delivered daily by each of the EOS satellites.

Files on JPL's server are selected by defining a geographic area as well as start and stop times. A list of all applicable data files is presented and individual six minute files can be downloaded. In order to have radiosonde wind profiles available to compare to the profiles derived from satellite soundings, locations for this project were selected from radiosonde sites that the Aqua satellite passed over near scheduled release times (00Z and 12Z). NASA's Earth Observatory website provides a Satellite Overpass

Predictor that, for any specified geographic location and selected satellite, lists overflight times and elevation angles. The format of the file generated by this software is shown in Figure 20.

```
Satellite #27424  : AQUA
Element Set Number: 506 (Orbit 40430)
Element Set Epoch : 09Dec09  13:58:25.757 UTC   (1.2 days ago)
Orbit Geometry    : 699.00 km x 700.23 km at 98.199 deg
Propagation Model : SGP4
Ground Location   : Anchorage, AK, USA
Time is shown in  : UTC (+0.00 h)


Wed  02Dec09  ---  Orbit 40329

   UTC    Azimuth  Elev    Range    Height  Sun Ang  V
           [deg]  [deg]     [km]     [km]    [deg]

12:44:28     8.7   52.9    868.6     681.6    77.2   N
12:44:48     4.1   61.8    797.0     682.0    68.7   N
12:45:08   353.8   71.6    746.5     682.4    59.1   N
12:45:28   319.5   80.4    721.6     682.8    48.6   N
12:45:48   249.1   78.8    725.0     683.2    38.5   N
12:46:08   223.9   69.4    756.3     683.6    29.8   N
12:46:28   215.6   59.7    812.3     684.1    23.8   N
12:46:48   211.7   51.1    888.2     684.6    21.3   N


Wed  02Dec09  ---  Orbit 40334

   UTC    Azimuth  Elev    Range    Height  Sun Ang  V
           [deg]  [deg]     [km]     [km]    [deg]

22:22:58   131.8   57.7    826.6     683.8   113.2   D
22:23:18   119.5   66.1    771.7     683.3   104.7   D
22:23:38    93.6   73.1    741.1     682.9    95.1   D
22:23:58    51.2   74.0    737.9     682.5    84.9   D
22:24:18    20.9   67.9    762.3     682.1    75.1   D
22:24:38     6.4   59.6    812.0     681.7    66.2   D
22:24:58   359.0   51.5    882.6     681.3    58.6   D
```

Figure 20. File Format Available Through NASA's Satellite Overpass Prediction Tool (NASA-Satellite Overpass Predictor)

Once identified, the appropriate file is downloaded and the necessary data sets are imported into MATLAB. The eight AIRS data sets imported for this research are:

Geolocation:	Sounder Data:
Latitude	TAirSup
Longitude	TAirSupError
Time	GP_Surface
	PSurfStd
	nSurfStd

The descriptions for each of these data sets are found in the AIRS Version 5.0 Released Files Description document. The applicable excerpts are shown in Table 4.1: (Jet Propulsion Laboratory, 2007)

Table 4.1 Excerpts from JPL AIRS Sounder Data File Description File

Geolocation Fields

These fields appear for every footprint (GeoTrack * GeoXTrack times) and correspond to footprint center coordinates and "shutter" time.

Name	Explanation
Latitude	Footprint boresight geodetic Latitude in degrees North (-90.0 ... 90.0)
Longitude	Footprint boresight geodetic Longitude in degrees East (-180.0 ... 180.0)
Time	Footprint "shutter" TAI Time: floating-point elapsed seconds since Jan 1, 1993

Along-Track Data Fields

These fields appear once per scanline (GeoTrack times).

Name	Type	Extra Dimensions	Explanation
TSurfAir	32-bit floating-point	None	Surface air temperature in Kelvins
TSurfAirErr	32-bit floating-point	None	Error estimate for TSurfAir
PSurfStd	32-bit floating-point	None	Surface pressure first guess in mbar, interpolated from forecast
nSurfStd	32-bit integer	None	Index in pressStd array of first pressure level above mean surface (1 ... 15)
GP_Surface	32-bit floating-point	None	Geopotential Height of surface (m above mean sea level)

Each data point corresponds to one of the 1350 sounding locations covered by the six-minute swath (45 points along the flight path, 30 points wide). The sounding coordinates for one of these data files, plotted on a Wolfram Mathematica cylindrical projection map, is shown in Figure 21. This file covers a segment of a descending pass that tracked along the eastern border of Alaska, and was used to derive a wind profile over a notional dropzone located at the rawinsonde release location at the Anchorage International Airport.

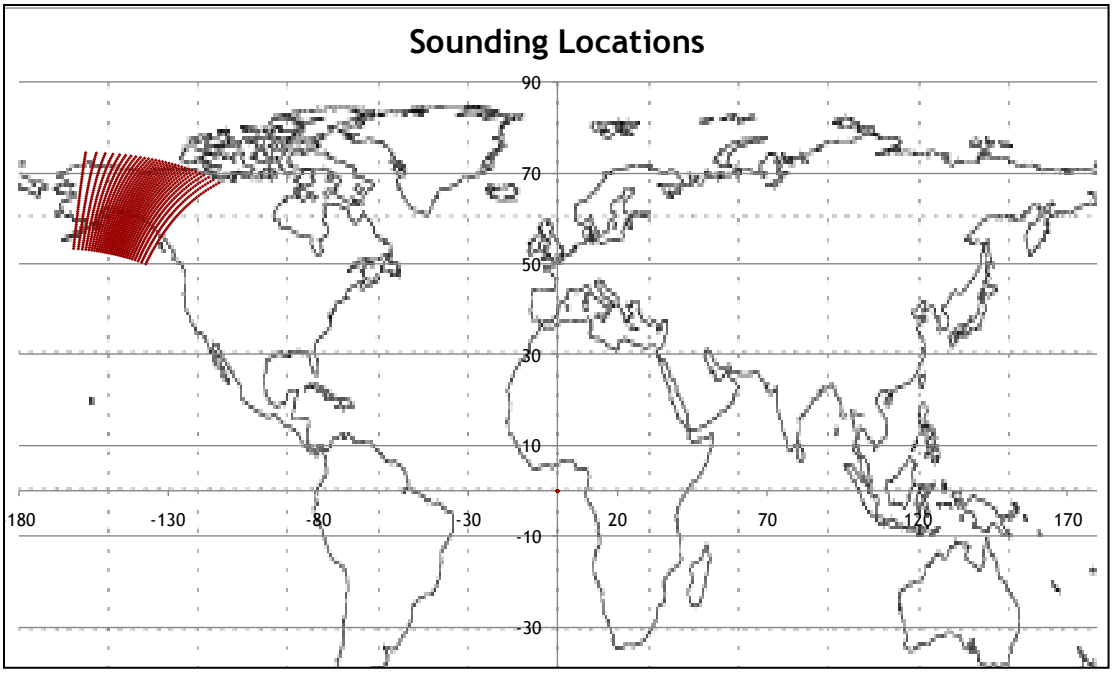

Figure 21. Depiction of Sounding Boresight Coordinates for a 6-Minute Data File

The TAirSup data set contains atmospheric temperature values for 100 vertical pressure levels at each sounding location. The pressure levels used to locate the measured temperatures are the same for each point, making it possible to compare one sounding location to another. The data set is filtered to collect vertical temperature profiles for the 200 sounding locations closest to the drop zone coordinates. Of the 100 pressure levels, only the 25 levels below the 500 mb level are of interest to this project. Filtering out the high altitude temperatures provides the data set used to derive the wind profile over the drop zone. This set consists of 200 geographic locations within about 300 km of the objective area. For each of these locations, the data set includes surface pressure, surface geopotential height, and a temperature measurement for up to 25 pressure levels between 500 mb and 1100 mb (all 25 temperatures may not be available due to terrain elevation and surface pressure). The algorithm calculating a temperature value from the satellite measured brightness temperatures assigns an error value to each

data point. A depiction of typical error values is presented in Figure 22 for one layer of a sounding data file (905 mb). In this research, temperature measurements with error exceeding 3 K were excluded.

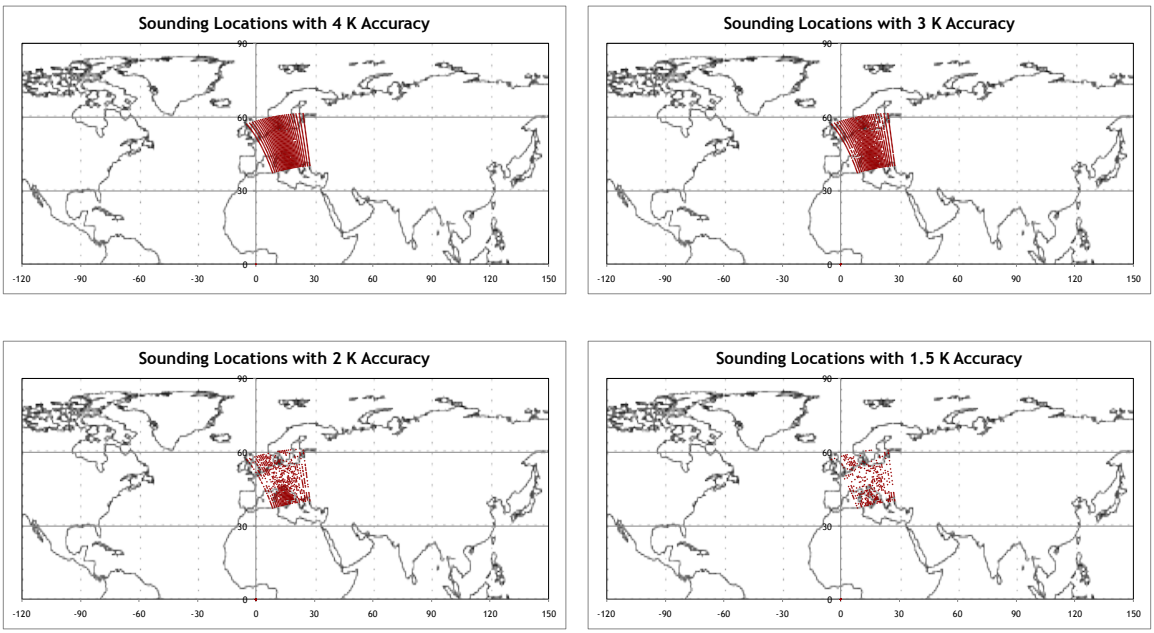

Figure 22. Soundings with Temperature Measurement Error Better Than Specified Tolerance

Derivation of Vertical Wind Profile

For each of these bottom 25 levels, cubic spline interpolation is used to fill in pressure and temperature values for all locations within 2 degrees of longitude and latitude from the drop zone coordinates. This 4x4 degree geographic region spans about 445 km north-south and between 200 and 400 km measured east-west for midlatitude locations (depending on the latitude). From this interpolated data, the slope of the constant pressure surface, as well as the rate of temperature change along the pressure level in both the east-west and the north-south direction can be determined. The thermal wind relationship is described in Equations 10 and 11 (Wallace & Hobbs, 2006):

$$(u_g)_2 - (u_g)_1 = -\frac{g_0}{f}\frac{\partial(Z_2 - Z_1)}{\partial y} \quad (10)$$

$$(v_g)_2 - (v_g)_1 = \frac{g_0}{f}\frac{\partial(Z_2 - Z_1)}{\partial x} \quad (11)$$

The thickness of each layer ($Z_2 - Z_1$) is linearly proportional to the temperature, as described by the hypsometric equation:

$$Z_2 - Z_1 = \frac{R_d \bar{T}_v}{g_o} \ln\left[\frac{p_1}{p_2}\right] \quad (12)$$

R_d is the dry gas constant and g_o is the acceleration due to gravity at the surface. The variable f is the Coriolis parameter, which depends on the latitude of the objective area. Combining these two equations provides a method of determining the vertical change in u and v components of the geostrophic wind through each layer. The change wind between the top and bottom of a pressure layer is only a function of the vertical change in pressure through the layer, and the horizontal temperature gradient.

$$(u_g)_2 - (u_g)_1 = \frac{R_d}{f} ln\left[\frac{p_1}{p_2}\right] \frac{\partial T}{\partial y} \quad (13)$$

$$(v_g)_2 - (v_g)_1 = \frac{R_d}{f} ln\left[\frac{p_1}{p_2}\right] \frac{\partial T}{\partial x} \quad (14)$$

This form of the thermal wind relationship from the Wallace and Hobbs text neglects the dependence on vertical temperature gradient, which also contributes to the wind gradient. Howard Bluestein, in *Synoptic-Dynamic Meteorology in Midlatitudes*, provides the more complete equations for the wind gradients by u and v components (Bluestein, 1992):

$$\frac{\partial u_g}{\partial z} = -\frac{g}{f\,T}\left[\left(\frac{\partial T}{\partial y}\right)_z + \frac{\partial T}{\partial z}\left(\frac{\partial z}{\partial y}\right)_p\right] \quad (15)$$

$$\frac{\partial v_g}{\partial z} = \frac{g}{f\,T}\left[\left(\frac{\partial T}{\partial x}\right)_z + \frac{\partial T}{\partial z}\left(\frac{\partial z}{\partial x}\right)_p\right] \quad (16)$$

IV. Results and Analysis

Validation of Satellite-Measured Temperatures

Because this project relies on accurate atmospheric temperature data, it is appropriate to validate the accuracy of the temperature obtained from satellite soundings. For multiple radiosonde launch locations, a comparison was made between radiosonde measured temperatures and the satellite measured temperature profile for the sounding location closest to the launch site. Agreement was typically very good, with average deviations between 1 and 2 K for each profile. The largest variation occurred in the lowest 2 to 3 pressure levels, where reported temperature error estimates greater than 10 K are common. An example comparison for a RAOB location in Stuttgart, Germany is shown in Figure 23.

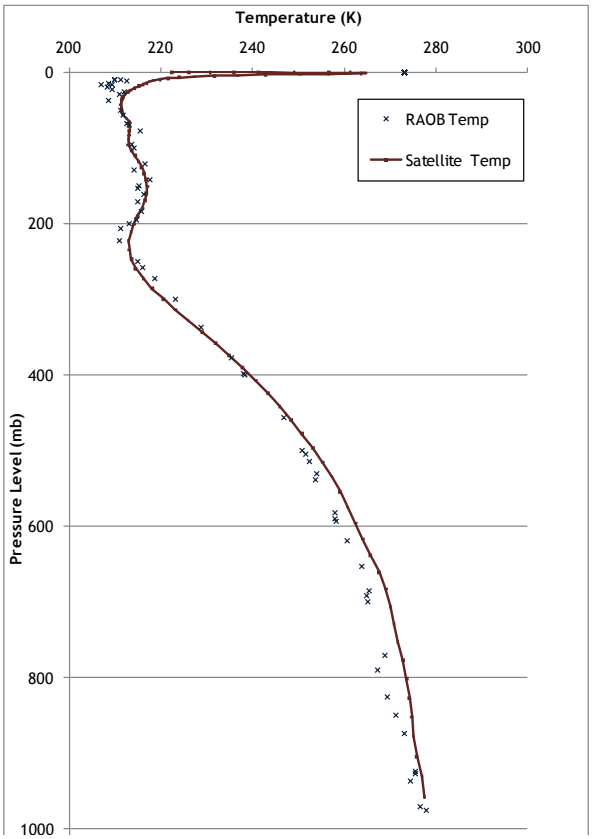

Figure 23. Comparison of RAOB and AIRS Temperatures. Stuttgart, Germany – 2 Dec 2009, 12Z

Lookup of Terrain Elevation for Each Sounding Location

The Level 2 data available from the Aqua satellite sounders provides the atmospheric pressure at the surface (by interpolation from forecast data) and the geopotential height of the surface in meters. The surface terrain elevation for each of these sounding locations is a potential starting point for assigning heights to each subsequent pressure level. The coarse elevation data required is available from many possible sources. This project uses the United States Geological Survey (USGS) Seamless Elevation data set, and to automate the lookup by latitude and longitude coordinates, the online Elevations Query by Zonum Solutions was utilized.

This software package accepts a list of up to 500 coordinates, and builds a corresponding list of elevation values by looking up each location in the USGS dataset. The values obtained were matched with the sounding locations to be used as the height of the bottom of the first pressure level. Figure 24 shows the current user interface.

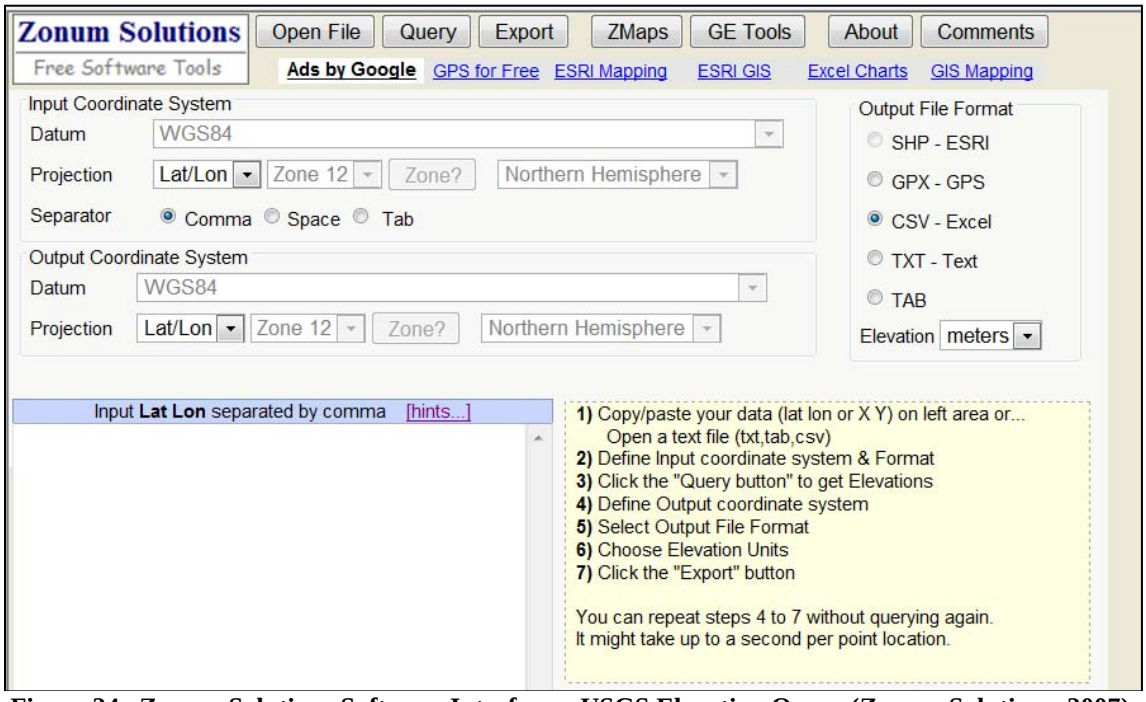

Figure 24. Zonum Solutions Software Interface – USGS Elevation Query (Zonum Solutions, 2007)

To confirm the accuracy of this method, a grid of 10,000 evenly spaced coordinates was created surrounding one of the test sounding locations (Anchorage International Airport, Alaska). Terrain elevation values were retrieved from the USGS data set and were plotted in MATLAB, as shown in Figure 25a. Figure 25b is a topographic chart from Johns Hopkins University Applied Physics Laboratory with the same geographic area highlighted. Terrain features match up well, and comparison of individual elevation levels confirmed that the method was correctly assigning surface elevation levels to lat/lon coordinates.

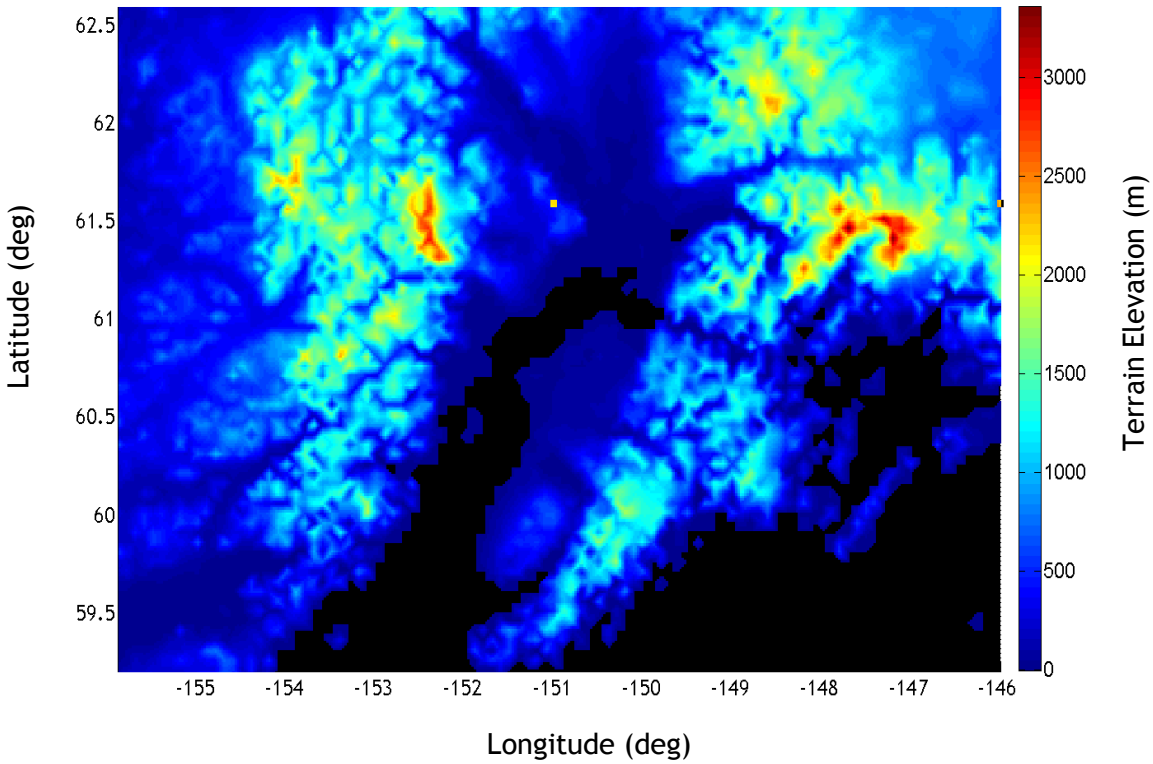

Figure 25a. Plotted USGS Elevation Values for Anchorage, AK Area

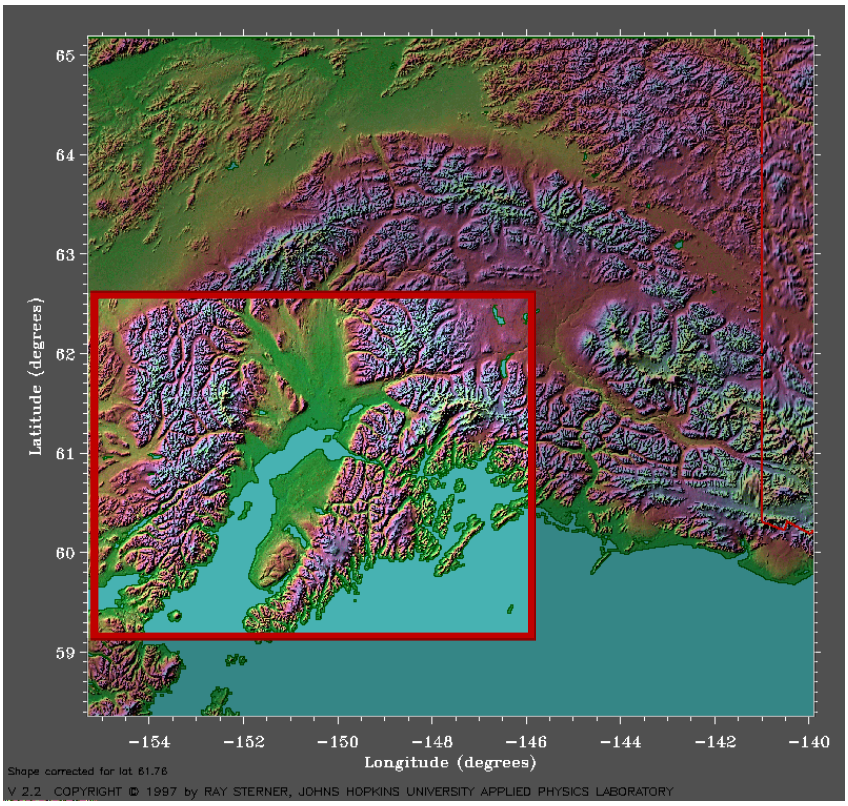

Figure 25b. Anchorage Area Topographic Map—Highlighted Area is the Geographic Region Covered by Plot in Figure 25a

Assignment of Heights to Pressure Levels

To determine the shape of each isobaric surface, the height of each pressure level within each vertical temperature profile must be determined. These heights can be calculated by first finding the thickness of each layer, and then adding them together. A known starting point is needed, and two approaches were used in this project—a bottom-up method, and a top-down method.

The thickness of a single layer is primarily a function of temperature, and can be calculated by the hypsometric equation (Wallace & Hobbs, 2006):

$$Z_2 - Z_1 = \frac{R_d \bar{T}_v}{g_o} \ln\left[\frac{p_1}{p_2}\right] \tag{17}$$

The mean virtual temperature, $\bar{T}_v$, is approximated by averaging the satellite measured temperatures at the top and bottom of the layer. Using the actual temperature instead of a virtual temperature neglects the moisture content of the air, which is a reasonable approximation because it is the only pressure and temperature gradients that are of interest. The moisture content of the air, while unknown, does not likely change very much from one grid point to the next, so neglecting it should have a similar effect on thickness at each grid point, and therefore not have a significant effect on the slope of the pressure surfaces. Figure 26 shows the variables used to determine the thickness of the lowest five data layers.

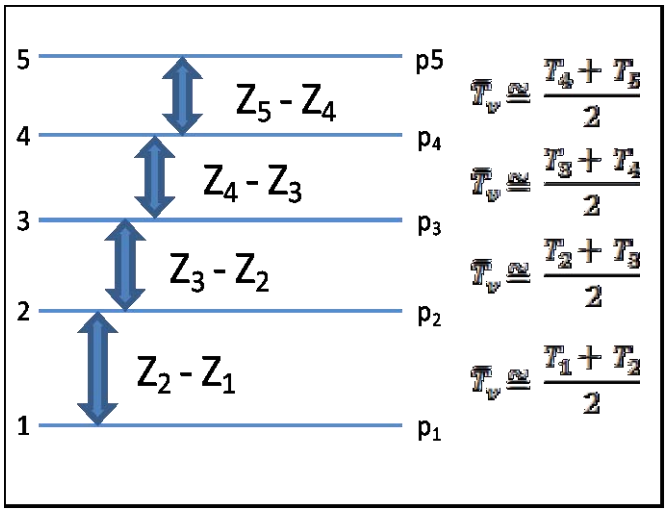

Figure 26. Determination of Thickness of Each Atmospheric Layer

The AIRS reported surface pressure will fall between two of the satellite's standard pressure levels. Starting with the surface elevation extracted from the USGS dataset, the hypsometric equation is used to assign a height above sea level to the first standard pressure level that is above the surface. From that height, each subsequent layer's thickness is calculated and added to assign the rest of the heights and create the pressure level height profile. Figure 27 shows the close correlation between these

calculated pressure level heights and rawinsonde-measured heights for a single sounding location.

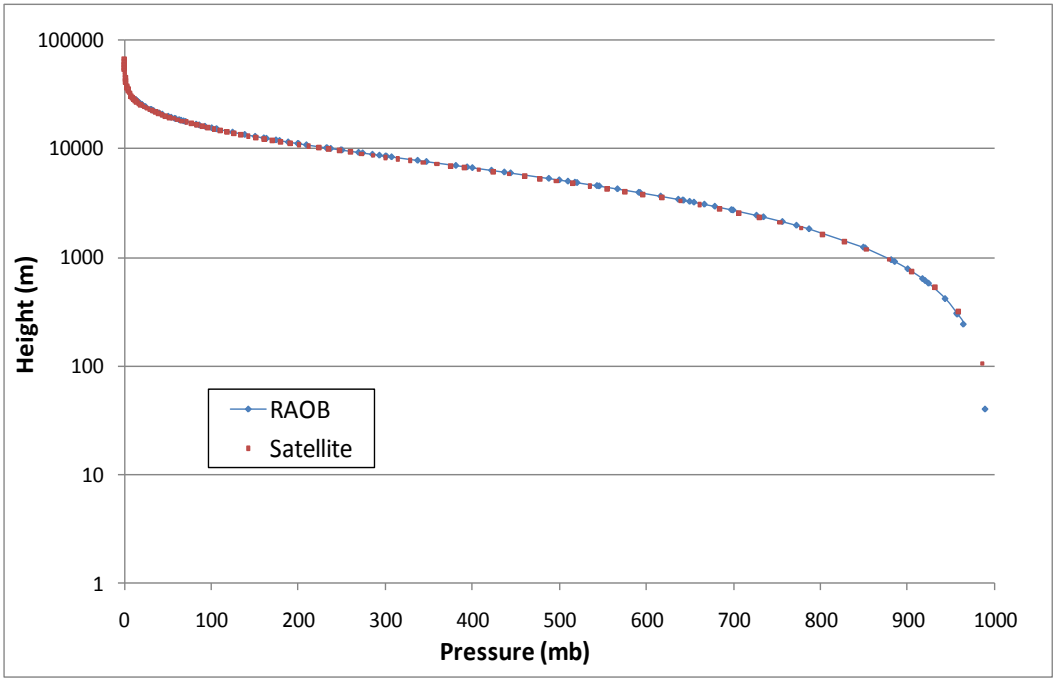

Figure 27. Calculated Heights Compared to Rawinsonde Observed (RAOB) Heights

The pressure surfaces obtained by combining multiple height profiles obtained by this bottom-up method do not appear realistic, showing steep pressure gradients in areas where GFS surfaces are almost flat. This is likely due to the fact that any small geolocation errors in regions of steep terrain could lead to large errors in surface elevation. Additionally the lowest pressure level temperatures are prone to larger error than higher altitude soundings, so relying heavily on them leads to error throughout the vertical profile. For these reasons, the top-down approach was used to create more accurate constant pressure surfaces.

Incorporation of Global Forecast System Data

For a starting point in this top-down method, GFS data is used. The 500 mb pressure level roughly corresponds to an altitude of 16,000 -18,000 feet above sea level,

making it a good choice for most JPADS airdrops. Many airdrops are conducted at or below this level, so accurately predicting the winds between 500 mb and the surface would validate the method. If needed for higher altitude airdrops, GFS data for a lower pressure level could be used as a starting reference point.

For this research, GFS 500 mb heights (an example is shown in Figure 28) are gridded, so that interpolated height values are available for each satellite sounding location. Then, the previous surface up method is reversed, using the hypsometric equation to first assign a height to the first AIRS data level below the 500 mb level, (the 516 mb level), and then to each lower pressure level until the surface is reached.

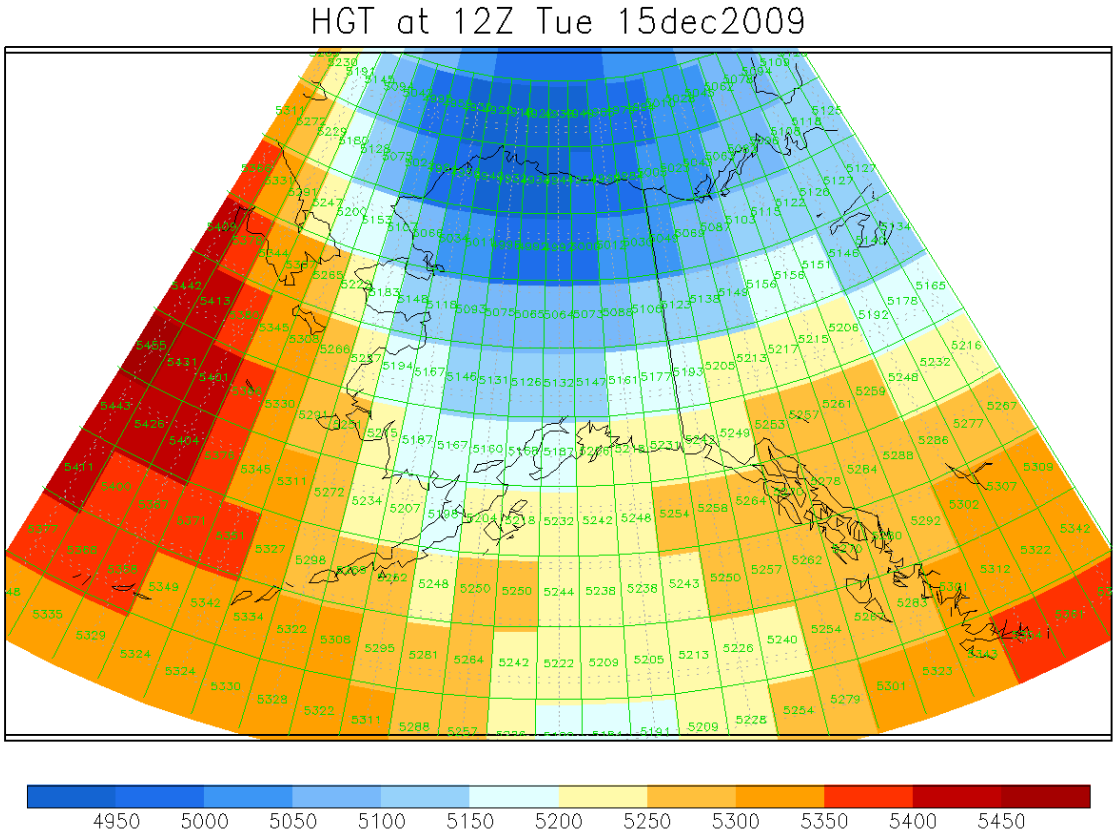

Figure 28. Global Forecast System 500 mb Geopotential Heights

The GFS heights are available on a grid with approximate spacing of 2.5 degrees of longitude and latitude. Of course, these grid points do not match the coordinates of the satellite sounding locations, so a method of interpolating between the GFS data must be used to calculate a 500 mb height at each sounding point. This was accomplished using the MATLAB *griddata* function, using cubic spline interpolation. The resulting isobaric surface for the 12Z, 15 Dec 2009 GFS data previously presented in Figure 28, is shown below in Figure 29.

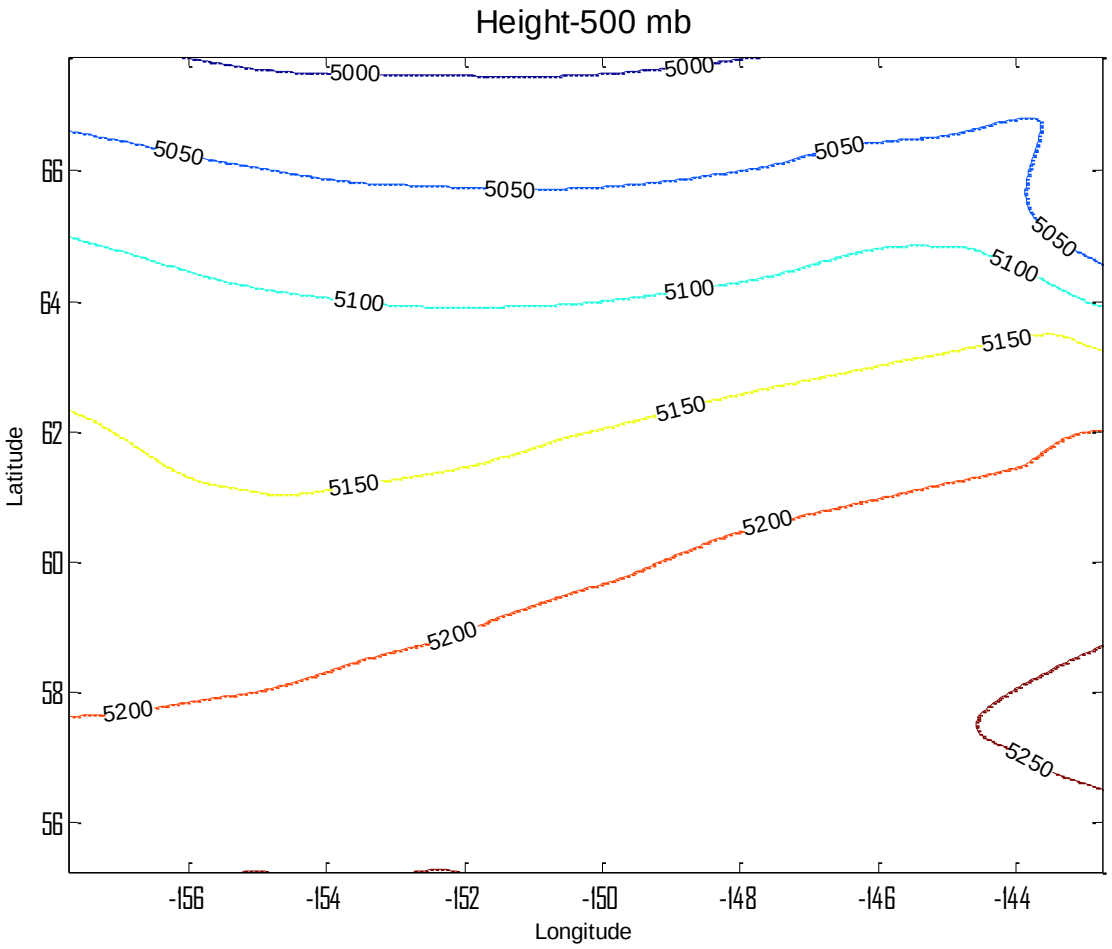

Figure 29. Gridded GFS 500 mb Geopotential Heights

Calculation of Isobaric Surfaces

For each of the 200 sounding locations closest to the dropzone coordinates, heights are assigned to each pressure level. Then, for each pressure level, all 200 heights are combined to build surfaces of constant pressure. Various methods were used to smooth the height data to minimize the effect of small variations caused by errors in the measured temperatures. Some of the unsmoothed height data sets contain multiple relative high and low pressure locations, but because the geographic region covered is only about 600-800 km across, this is not likely. For that reason, each layer of the data set was smoothed by fitting a third order, three-dimensional polynomial surface to the temperatures and heights in each pressure level. This limited the surface to have no more than one relative minimum and maximum height across the region of interest.

Figures 30 and 31 illustrate, in two dimensions, the smoothing process. Figure 30 shows two vertical cross-sections through a sounding data set. The blue data points show a column of sounding locations parallel to the flight path of the satellite and the red locations are an east-west row perpendicular to satellite track. The intersection of the two lines is the location of the notional dropzone.

In Figure 31, the temperature measurements within the 905mb layer for each sounding location along these two lines is plotted. The small error and variation in the temperatures can lead to many different values for temperature gradient, depending on how many data points are included, and how a curve is fit to the data. In Figures 31a and 31b, the location of the dropzone in each cross-section is indicated by the orange triangle.

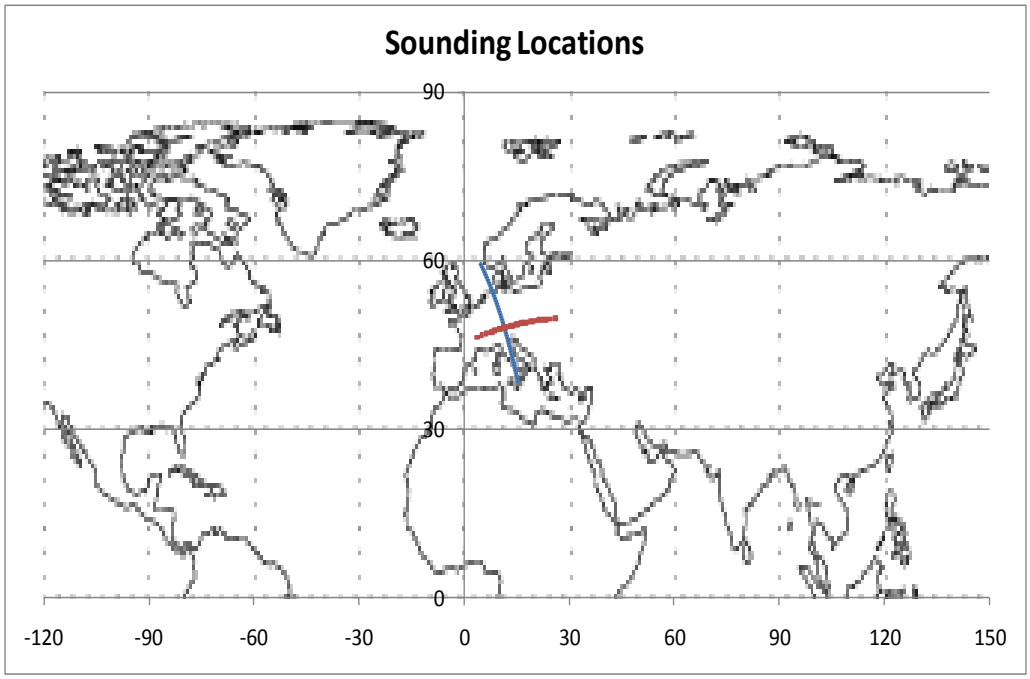

Figure 30. Sample of Sounding Locations Surrounding Dropzone--Along Satellite Flight Path (blue) and Perpendicular to Satellite Flight Path (red)

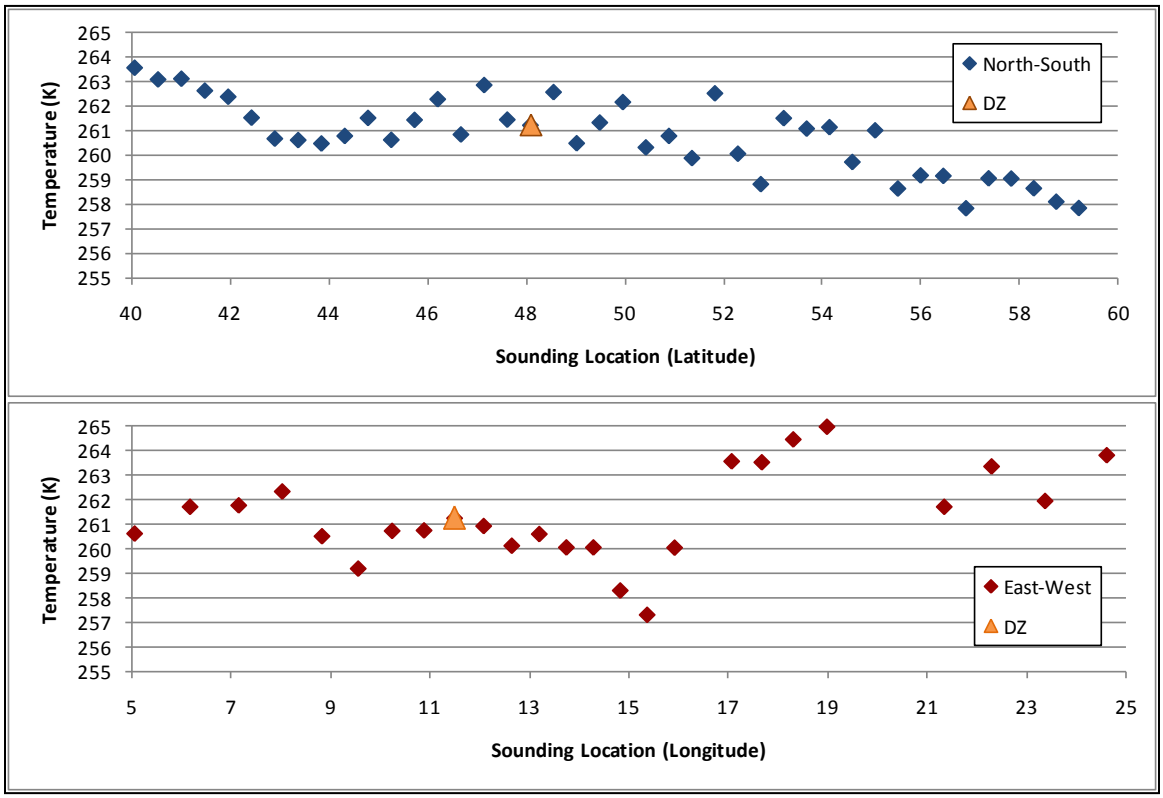

Figure 31a. Satellite Measured Temperature Values Along Satellite Flight Path (blue) and Perpendicular to Satellite Flight Path (red)

To smooth the data, and calculate the most accurate temperature and height gradients, the 200 data points closest to the dropzone were selected, and all data farther from the dropzone was neglected. A three-dimensional surface was fit to this data by least squares regression for each layer. Cross-sections of this surface are shown in Figure 31b. The slope of this surface at the dropzone coordinates is used as the temperature gradient, and by a similar curve fitting process the pressure gradient in each layer is determined. This method of smoothing accounts for more data points than just the few immediately surround the dropzone coordinates, and minimizes the effect of error in the satellite measured temperatures.

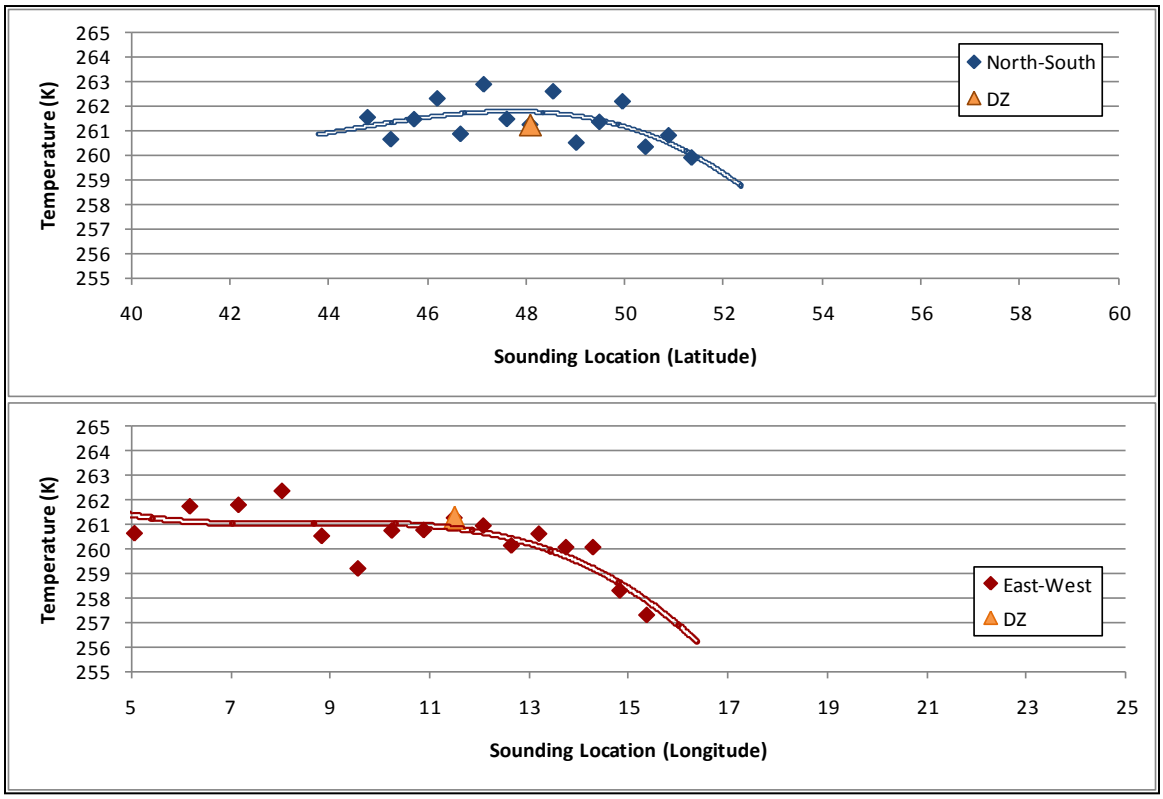

Figure 31b. Cross-sections of Smoothed Surface fit to Temperature Measurements Surrounding Dropzone Location

Figure 32 shows twenty of these isobaric surfaces over a notional drop zone located in Munich, Germany, 12Z on 10 Jan 2010. The dropzone coordinates are in the center of the geographic area covered by these plots. The slope of the pressure surfaces at the midpoint and the temperature gradient within each isobaric surface are used to derive the wind at each layer's altitude.

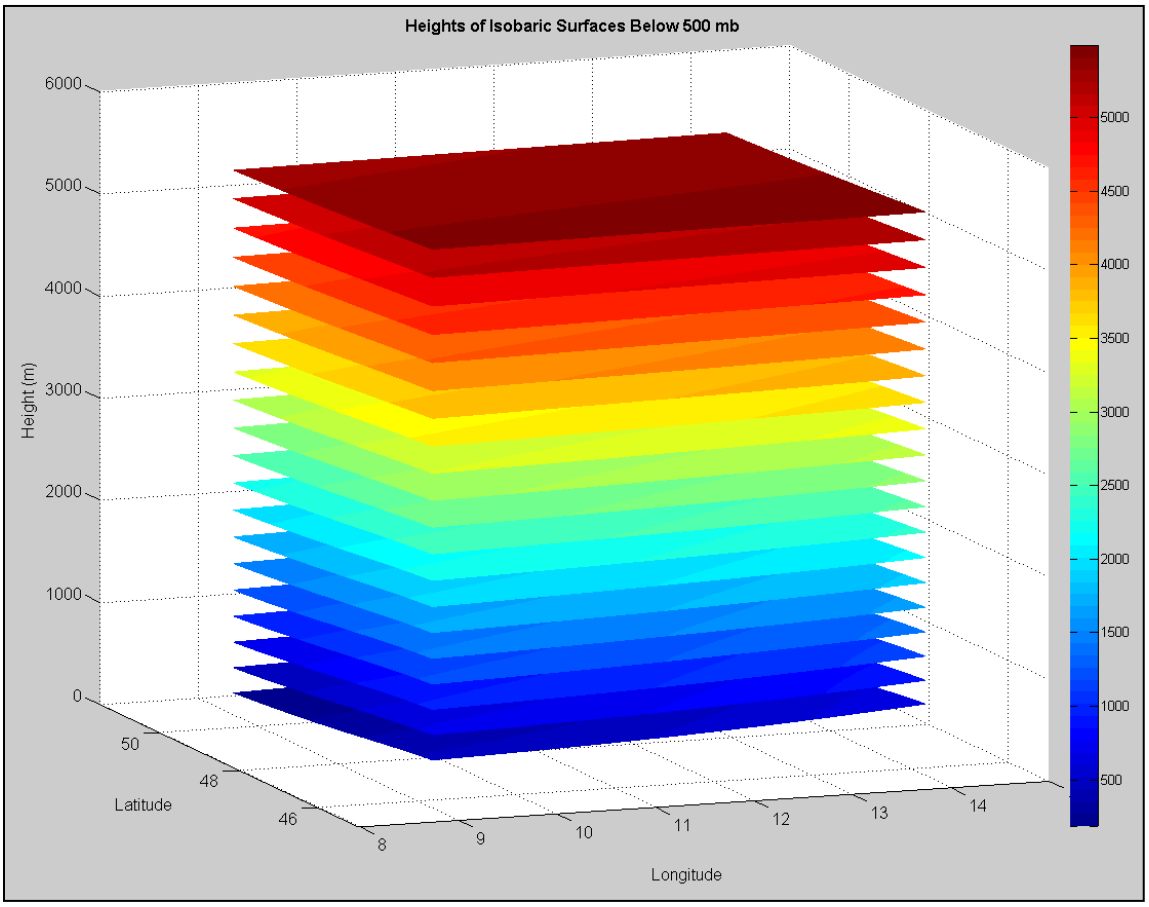

Figure 32. Isobaric Surfaces Calculated from Satellite-Derived Layer Thicknesses

This same set of data is presented in Figure 33 in a more useful format, as a series of contour plots. The x and y axes for each of the subplots are longitude and latitude respectively (with the dropzone coordinates in the center of the plot). The contours show the height, in meters, for the pressure level listed above each plot.

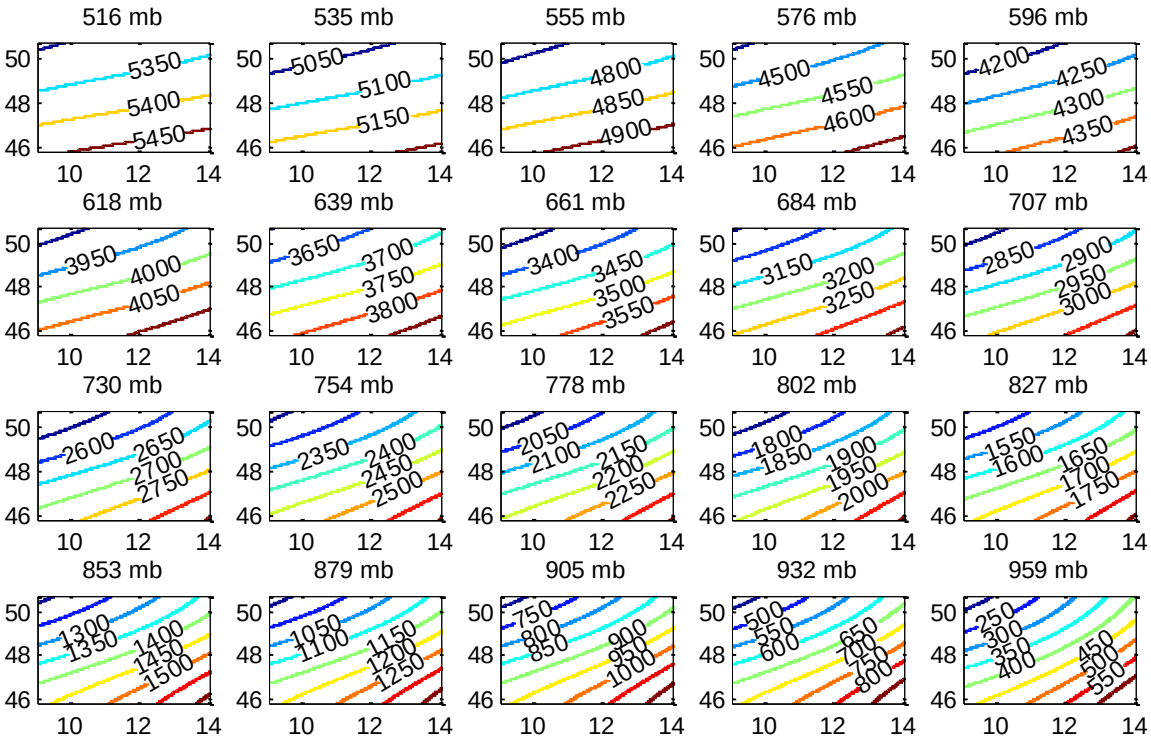

Figure 33. Geopotential Height Contours by Latitude and Longitude (Munich, GE—7 Jan 10, 12Z)

Determination of Temperature Gradients in Each Pressure Level

Within each of these pressure levels, the measured temperatures are smoothed to create a temperature distribution. At the center of each temperature surface, the rate of change in temperature in both the x and y directions are calculated. The vertical temperature gradient is found by dividing the difference in temperature at the center of two pressure surfaces by the vertical separation between the surfaces. The temperature distributions corresponding to the pressure levels in Figure 33 are plotted in Figure 34.

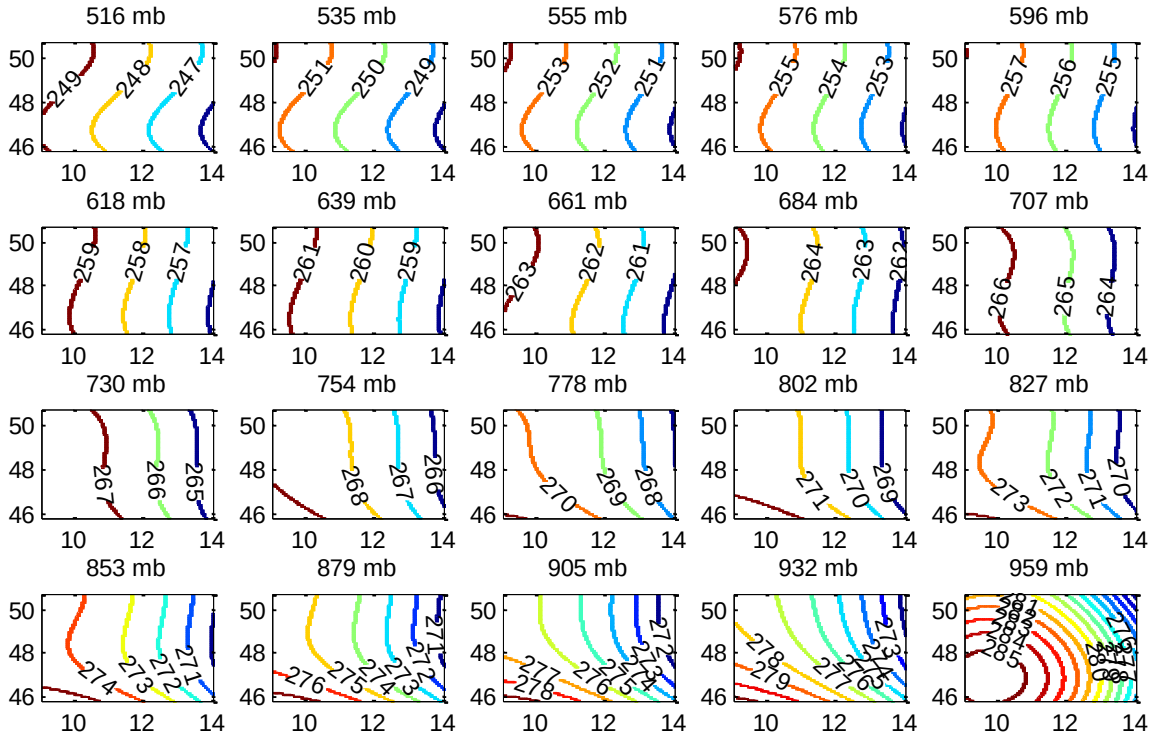

Figure 34. Temperature Distribution within Isobaric Surfaces-Plotted by Latitude and Longitude (Munich, GE—7 Jan 10, 12Z)

Derivation of the Vertical Wind Profile

Using the methods detailed in Chapter 3, the pressure and temperature gradients above the dropzone at each pressure level are used to derive the geostrophic wind and thermal wind. The temperature and pressure gradients calculated for the notional dropzone location near Munich, Germany, (the data set previously presented in Figures 30 through 34), are listed in Table 4.2.

Table 4.2 Calculated Pressure and Temperature Gradients by Pressure Level

Pressure			From Satellite Heights		From Satellite Temps		
Level	Temp	dZ	dH/dx	dH/dy	dT/dx	dT/dy	dT/dz
(mb)	(K)	(m)			(K/m)	(K/m)	(K/m)
500.00							
515.72	249.55	277.21	0.0001350	-0.0002661	-9.1801E-06	1.1321E-06	-0.008371
535.23	251.85	279.10	0.0001454	-0.0002673	-9.4740E-06	1.0330E-06	-0.008079
555.17	254.06	277.27	0.0001728	-0.0002814	-9.6739E-06	8.5316E-07	-0.007772
575.52	256.16	275.35	0.0002002	-0.0002952	-9.8520E-06	6.2191E-07	-0.007025
596.31	257.93	273.33	0.0002277	-0.0003088	-9.9593E-06	4.3312E-07	-0.006917
617.51	259.94	271.31	0.0002551	-0.0003224	-9.9785E-06	5.6809E-07	-0.007353
639.14	261.92	269.49	0.0002821	-0.0003361	-9.6067E-06	6.1046E-07	-0.007776
661.19	264.13	267.61	0.0003086	-0.0003498	-9.2757E-06	6.3478E-07	-0.006852
683.67	265.59	265.42	0.0003347	-0.0003633	-9.0495E-06	2.4838E-07	-0.005160
706.57	266.87	262.97	0.0003605	-0.0003764	-8.9185E-06	-2.7456E-07	-0.004982
729.89	268.21	260.66	0.0003862	-0.0003889	-8.9471E-06	-9.6589E-07	-0.006008
753.63	270.00	258.52	0.0004117	-0.0004008	-9.0176E-06	-1.3697E-06	-0.006089
777.79	271.36	256.33	0.0004373	-0.0004123	-9.1754E-06	-2.0299E-06	-0.005247
802.37	272.69	254.04	0.0004631	-0.0004235	-9.9812E-06	-2.0801E-06	-0.004998
827.37	273.90	251.85	0.0004897	-0.0004347	-1.0910E-05	-2.0987E-06	-0.005662
852.79	275.54	249.77	0.0005170	-0.0004457	-1.2102E-05	-2.4745E-06	-0.006124
878.62	276.96	247.73	0.0005452	-0.0004560	-1.3199E-05	-3.8524E-06	-0.005692
904.87	278.36	248.09	0.0005743	-0.0004650	-1.4331E-05	-5.5140E-06	-0.028813
931.52	291.32	247.88	0.0006075	-0.0004698	-1.7125E-05	-6.5785E-06	-0.028813

In many cases the direction of the geostrophic wind, which is parallel to the height contours at each level, is close to the wind direction measured by the rawinsonde. Large deviations occur however when this method of building pressure surfaces is used to predict the magnitude of the wind. The derived wind shown in Figure 35 is typical of these results, where even the initial trend in wind speed is in the incorrect direction. The geostrophic wind speed is proportional to the steepness of the isobaric surface. For this 7 Jan, 2010 sounding near Munich, Germany, the height contours become closer together with each lower altitude level, leading to the increasing wind speed. The radiosonde, however, measured a mostly constant wind speed down to the 750 mb level, and then a decrease in wind speed throughout the boundary layer.

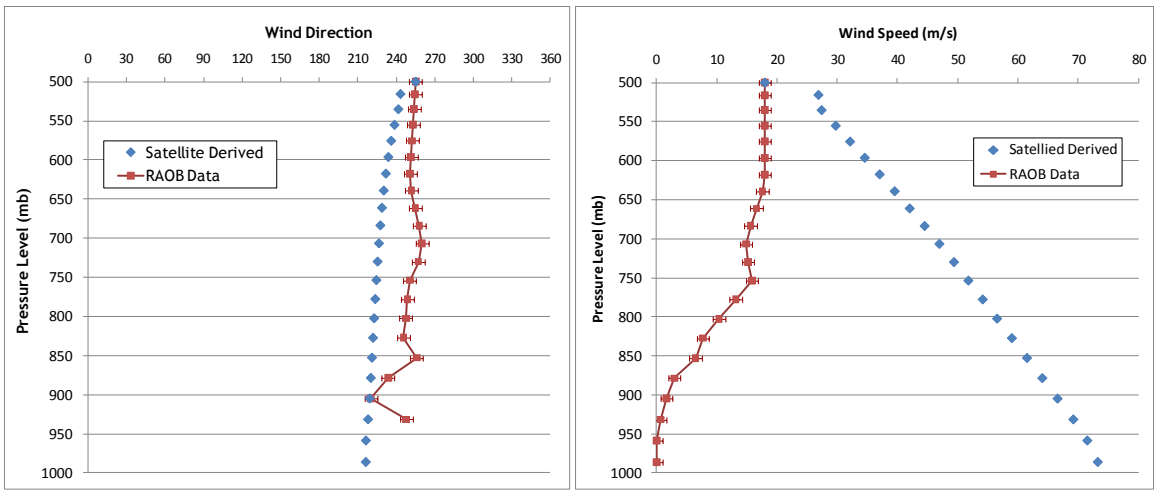

Figure 35. Comparison of Derived Geostrophic Wind with RAOB (Munich, GE—7 Jan 10, 12Z)

More accurate winds were predicted by using the thermal wind equation to modify the geostrophic wind profile. As Figure 36 shows, in the case of the Munich, Germany sounding, the derived wind direction more closely matches the RAOB. In addition, using the temperature gradients directly leads to a wind speed profile that is very similar to the RAOB between 500 mb and 750 mb. As with the geostrophic wind profile, the correct decrease in wind speed within the boundary layer is not predicted.

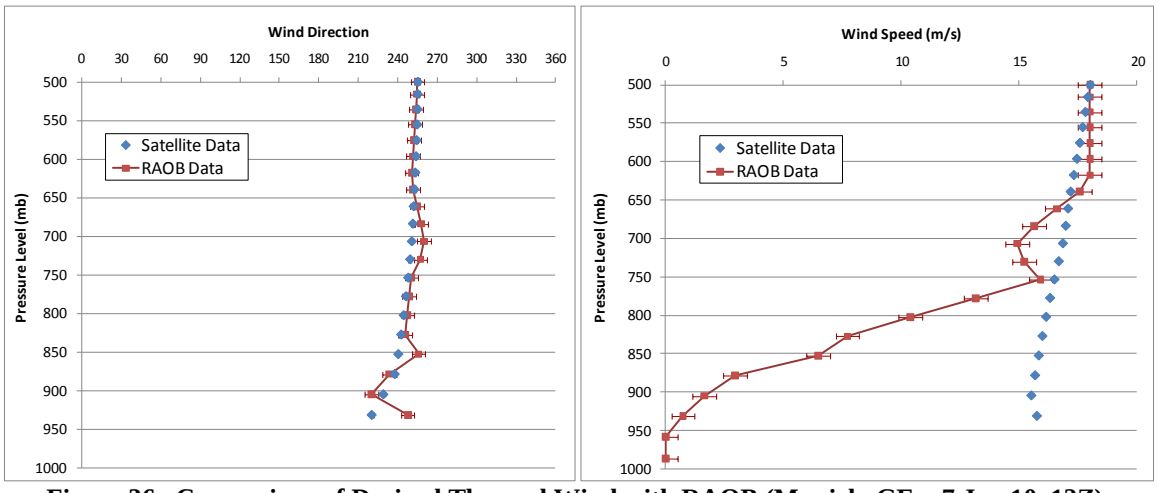

Figure 36. Comparison of Derived Thermal Wind with RAOB (Munich, GE—7 Jan 10, 12Z)

Ekman Spiral Boundary Layer Wind Profile

One approach to improve the lower portion of the wind profile is to combine it with a boundary layer wind model. The Ekman Spiral is a wind profile that makes the assumption that turbulent eddies throughout the boundary layer are constant with height. The wind at the top of the boundary layer is set to the geostrophic wind, and at the bottom of the boundary layer the wind magnitude is set to zero (or more accurately, could be spliced to a logarithmic wind profile within the surface layer). Because of the Coriolis Effect, the reduction in wind speed in the lower portion of the boundary layer leads to a change in the direction of the wind, as depicted in Figure 37.

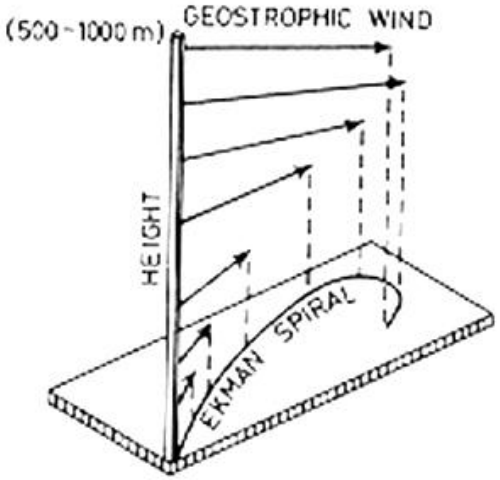

Figure 37. Depiction of the Ekman Spiral Wind Profile in the Boundary Layer (University of Virginia, 2010).

The set of equations that defines the wind in the Ekman Layer are:

$$K\,\frac{\partial^2 u}{\partial z^2} + f\left(v - v_g\right) = 0 \tag{18}$$

$$K\,\frac{\partial^2 v}{\partial z^2} - f\left(u - u_g\right) = 0 \tag{19}$$

This provides a method of further improving the satellite-derived wind profile. If the magnitude of the satellite predicted wind at each layer is multiplied by the fraction of the Ekman wind at that layer divided by the Ekman wind at the top of the boundary layer, a realistic boundary layer wind profile results. This correction, applied to the Munich, GE data, predicts the wind profile shown in Figure 38. In this initial investigation of the technique, the Ekman direction was not incorporated, because the previous method seems to accurately predict wind direction, and the Ekman direction depends on surface roughness, which adds an additional factor required for wind calculation.

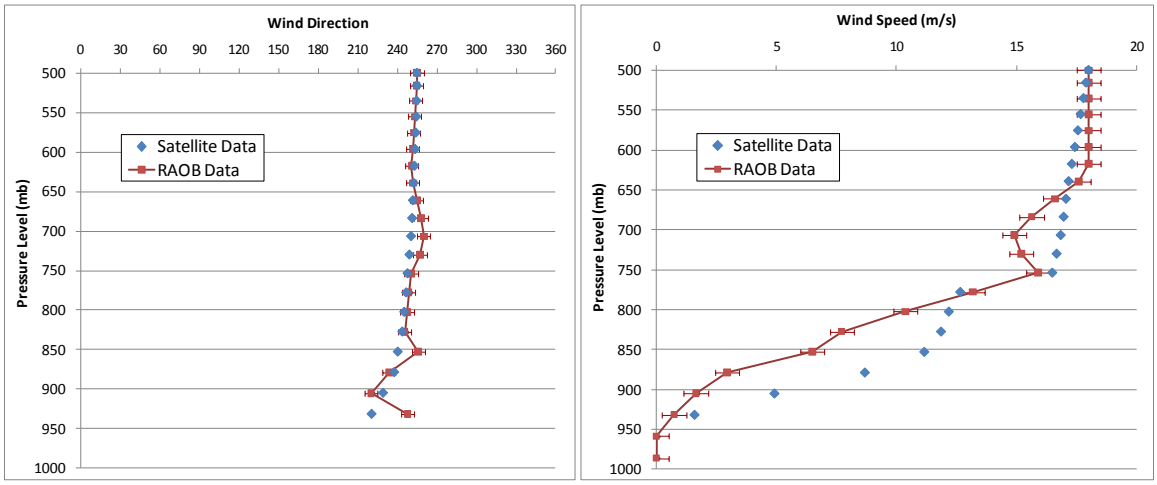

Figure 38. Thermal Wind with Ekman Spiral Speeds Below 800mb (Munich, GE—7 Jan 10, 12Z)

Comparison to GPS Dropsonde Performance

For a satellite update to eliminate the need for a GPS dropsonde, the accuracy of the derived wind profile needs to be comparable to the accuracy of the dropsonde. QinetiQ North America, the contractor currently responsible for the JPADS GPS dropsonde program, specifies performance as +/- 0.5 m/s for wind speed and +/- 1 degree for wind direction (QinetiQ-North America, 2008). If the accuracy of the satellite wind

profile is comparable, it could replace the dropsonde in all situations where reception of the satellite data is available. The actual wind profile accuracy required for a specific mission depends on the type of airdrop load, the size of the planned drop zone, and the drop altitude required by the threat environment.

V. Discussion

Conclusions

This project illustrates the potential for satellite-derived wind profiles to be used to make combat JPADS airdrops safer, while retaining the accuracy necessary to allow resupply to small dropzones. The method of combining calculated geostrophic wind and thermal wind profiles does a reasonable job determining the wind vector above the boundary layer. With some improvements to the low altitude wind profile modeling and expansion to use IR sounder data from additional polar-orbit satellites, this technique could be used in the near future to expand high altitude airdrop capabilities in the CENTCOM AOR.

Because wind speed generally increases with height, it is the higher altitude, free atmosphere winds that have the greatest effect on airdrop load drift. The strength of the method derived in this research is that it most reliably predicts the winds at the altitudes where knowing them is most important. As an example, for an airdrop from an altitude of 16,000 ft AGL, the portion of the atmosphere that the airdrop load will fall through that is above the boundary layer may only be about 70%, but the winds in that portion of the atmosphere could account for 85% or more of the drift effect on the airdrop load.

Satellite-Derived Wind Profile Advantages

The most important reasons to pursue this solution are the advantages it has over alternative wind update solutions. If the method can be improved to the point that the satellite-derived wind profile is as good as the dropsonde measured wind, the need for the potentially hazardous dropsonde pass through the objective area can be eliminated. The single pass solution saves the cost of the dropsonde, shortens the airdrop mission flight

time by 20-30 minutes, and prevents the aircraft from having to fly over the same terrain twice in a combat environment.

Other key advantages of the satellite wind solution include the fact that sensing the winds from space is completely passive. There are no emissions to be detected, or other indications that would identify the intended objective area prior to the airdrop. If existing communications methods are used to relay updated wind profiles to aircrew, using satellite-derived winds does not require any additional equipment to be installed on the aircraft conducting the airdrop. In addition, this method would not require a significant change in aircrew procedures nor require any additional training or equipment for ground forces.

One last advantage of satellite-derived winds versus dropsondes is that there is no dependence on GPS availability. Interference or jamming which interrupts the GPS signal during the time of fall of the dropsonde would prevent the dropsonde from accurately measuring the wind. At that point, crew options would be to release another dropsonde, abort the mission, or accept the greater potential for error and drop based only on the preflight forecast.

Recommendations for Future Research

Follow-on research in several areas could enhance the operational utility of this method. The first of these would be to expand the model to more accurately predict the wind within the boundary layer. Splicing the satellite-derived wind at the top of the boundary layer to an Ekman spiral wind profile, possible tied to the reported surface wind speed, will improve the overall accuracy of most profiles, and would lead to an integrated drift effect that is closer to reality. These approaches would account for the effect of

surface friction, and would create profiles with lighter winds in the boundary layer. An additional challenge with these techniques would be to accurately determine the height of the top of the boundary for each location because the thickness of the boundary layer varies greatly with location, time of day and time of year. It may also be possible to use satellite measured boundary level temperature in a more sophisticated weather model to even more accurately account for surface friction and come up with a better wind profile.

Also, as additional IR sounders are placed in orbit, the increased coverage and improvements in resolution will further enhance the availability and accuracy of derived wind profiles. Different satellites and sounders often provide data in different formats, so research should be conducted to adapt this wind derivation method to these new sources of atmospheric temperature.

This research demonstrates a method to predict wind profiles in areas with thin clouds, or no cloud cover. Microwave sounders on polar orbiting satellites provide data that could be used in a similar way to derive winds in cloud covered regions, with the disadvantage of less resolution than the infrared data. A third source of winds is winds determined by cloud feature tracking, using geostationary satellite images. By combining these three methods, winds profiles could be derived for more locations, with various levels of cloud cover. This would lead to a more flexible, operationally useful product, enabling in most situations, the single-pass airdrop.

Appendix A: List of Acronyms

AAA	Anti-Aircraft Artillery
AIRS	Atmospheric Infrared Sounder
AGU	Airborne Guidance Unit
AFIT	Air Force Institute of Technology
AFRL	Air Force Research Lab
AFWA	Air Force Weather Agency
AGAS	Affordable Guided Parachute System
AGL	Above Ground Level
AMC	Air Mobility Command
AMSU	Advanced Microwave Sounding Unit
AOR	Area of Responsibility
CARP	Computed Air Release Point
CDS	Container Delivery System
CENTCOM	Central Command
CONEMP	Concept of Employment
CTII	Combat Track II
DMSP	Defense Meteorological Satellite Program
EOS	Earth Observing System
EUMETSAT	Organisation for the Exploitation of Meteorological Satellites
GDAS	Global Data Assimilation System
GOES	Geostationary Operational Environmental Satellite
GFS	Global Forecast System
GPS	Global Positioning System
GRIB	Gridded Binary

GSI	Gridpoint Statistical Interpolation
HARP	High Altitude Release Point
HDF	Hierarchical Data Format
HVCDS	High Velocity Container Delivery System
IASI	Infrared Atmospheric Sounding Interferometer
I-CDS	Improved Container Delivery System
IED	Improvised Explosive Device
JPADS	Joint Precision Air Drop System
JPADS-MP	Joint Precision Air Drop System-Mission Planner
JPL	Jet Propulsion Laboratory, California Institute of Technology
LAR	Launch Acceptability Region
LIDAR	Light Direction and Ranging
MAF	Mobility Air Forces
MANPAD	Man Portable Air Defense System
METEOSAT	Meteorological Satellite
MetOp	Meteorological Operational
MSL	Mean Sea Level
NOAA	National Oceanic and Atmospheric Administration
PADS	Precision Air Drop System
RAOB	Rawinsonde Observation
RDF	Radio Direction Finding
RPG	Rocket Propelled Grenade
UAV	Unmanned Aerial Vehicle
USGS	United States Geological Survey

Appendix B: MATLAB Code

```
% Import AIRS Sounding Data File
% Maj. David C Meier
% AFIT/ENP
% 20 Oct 09
%

clc; % Clear the screen

csvwrite('Longitude.csv',Longitude)
csvwrite('Latitude.csv',Latitude)
csvwrite('Time.csv',Time)

csvwrite('Press.csv',pressSupp)
csvwrite('Temp.csv',TAirSup)

csvwrite('QualTempBottom.csv',Qual_Temp_Profile_Bot)
csvwrite('TempError.csv',TAirSupErr)

csvwrite('GP_Surf.csv',GP_Surface)
csvwrite('PSurfStd.csv',PSurfStd)
csvwrite('nSurfSup.csv',nSurfSup)
```

```
% Interpolate 500mb Heights for Sounding Locations from GFS Data
% Maj. David C Meier
% AFIT/ENP
% 15 Dec 09
%

%%  Initialize File

close all;
clear all;
clc;

%%  Import .xls data file with GFS Heights and Coordinates to
Interpolate

[numeric, text, raw]=xlsread('GFS_HGT.xlsx');
lon= numeric(1:42,1);
lat= numeric(1:42,2);
height= numeric(1:42,3);
range= numeric(1:6,4);

lon2= numeric(1:100,5);
lat2= numeric(1:100,6);

%%  Setup Parameters

left=min(lon);
right=max(lon);
bottom=min(lat);
top=max(lat);

dzlat=range(5);
dzlon=range(6);

%%  Grid Definition
xx=201;
yy=301;
x=linspace(left,right,xx);
y=linspace(bottom,top,yy)';

GFS(:,1) = lon;
GFS(:,2) = lat;
GFS(:,3) = height;

heightgrd = griddata(lon,lat,height,x,y,'cubic');

[C,h] = contour(x,y,heightgrd);
clabel(C,h)
title('Height-500 mb')

%%  Create Output File
```

```
newHGT(:,1) = lon2;
newHGT(:,2) = lat2;

%%  Interpolate for 500mb Heights at Sounding Locations

for count = 1:200

[a,xindex]=min(abs(x-lon2(count)));
[a,yindex]=min(abs(y-lat2(count)));

newHGT(count,3) = heightgrd(yindex,xindex);

end

csvwrite('InterpolatedHeights.csv',newHGT)
```

```
% Build Temperature and Pressure Surfaces from AIRS Data
% Maj. David C Meier
% AFIT/ENP
% 20 Oct 09

%%  Initialize File

close all;
clear all;
clc;

%%  Import .xls data file

 [numeric, text, raw] = xlsread('DataByLayer.xlsx');
lon = numeric(1:200,1);
lat = numeric(1:200,2);

temp = numeric(1:200,4);
height = numeric(1:200,5);

range = numeric(:,7);

%%   Define Geographic Boundaries

left=range(3);
right=range(4);
bottom=range(1);
top=range(2);

dzlat=range(5);
dzlon=range(6);
nlayers = range(7);

plevels = [515.7 535.2 555.2 575.5 596.3 617.5 639.1 661.2 683.7 706.6
729.9 753.6 777.8 802.4 827.4 852.8 878.6 904.9 931.5 958.6 986.1
1014.0 1042.2 1070.9 1100.0];

%%   Grid Definition

xx=201;
yy=301;

midptx=(xx+1)/2;
midpty=(yy+1)/2;

x=linspace(left,right,xx);
y=linspace(bottom,top,yy)';

%%   Fit Surface to Heights for Top (515.7mb) Pressure Level
fithgt = polyfitn...
    ([lon,lat],height,'constant x y x^2 y^2 x^3 y^3');% x^4 y^4')
    %Define surface to fit to height data
```

```
[ew, ns] = meshgrid(x,y);
zz = polyvaln(fithgt,[ew(:),ns(:)]);
zz = reshape(zz,yy,xx);

%%   Fit Surface to Temperatures for Top (515.7mb) Pressure Level
fittemp = polyfitn...
    ([lon,lat],temp,'constant x y x^2 y^2 x^3 y^3');% x^4 y^4')
    %Define surface to fit to temp data

[ew, ns] = meshgrid(x,y);
tt = polyvaln(fittemp,[ew(:),ns(:)]);
tt = reshape(tt,yy,xx);

%%   Plot Smoothed Surface

subplot(5,5,1)  %Set up to plot 5x5
contours=30;  %Maximum number of contours to plot

%lowestcountour = floor(min(height)/50)*50; %Lowest Geopotential Height
lowestcountour = floor(min(temp)); %Lowest level for temperature

%countourspacing=50;  %Contour Spacing for Geopotential Height
countourspacing=1;  %Contour Spacing for temperature

j=lowestcountour:countourspacing:lowestcountour+(contours*countourspaci
ng);

%[C,h] = contour(ew,ns,zz,j);  %Plot height contours
[C,h] = contour(ew,ns,tt,j);  %Plot temp surfaces

clabel(C,h)
title([int2str(plevels(1)),' mb'])

%%  Calculating size of each increment using spherical law of cosines
R=6371000;  %radius of earth in meters

xinc = R/(xx-1) *
acos(sind(dzlat)*sind(dzlat)+cosd(dzlat)*cosd(dzlat)*cosd(right-left));
yinc = R/(yy-1) *
acos(sind(bottom)*sind(top)+cosd(bottom)*cosd(top)*cosd(dzlon-dzlon));

%%  Calculating Rates of Height Change at DZ Coordinates

dhdx1=polyvaln(fithgt,[x(midptx+1),y(midpty)])-
polyvaln(fithgt,[x(midptx),y(midpty)]);
dhdx2=polyvaln(fithgt,[x(midptx),y(midpty)])-polyvaln(fithgt,[x(midptx-
1),y(midpty)]);

dhdy1=polyvaln(fithgt,[x(midptx),y(midpty+1)])-
polyvaln(fithgt,[x(midptx),y(midpty)]);
```

```
dhdy2=polyvaln(fithgt,[x(midptx),y(midpty)])-
polyvaln(fithgt,[x(midptx),y(midpty-1)]);

rate(1,1) = (dhdx1 + dhdx2)/(2*xinc);
rate(1,2) = (dhdy1 + dhdy2)/(2*yinc);

%%   Calculating Rates of Temp Change at DZ Coordinates

dtdx1=polyvaln(fittemp,[x(midptx+1),y(midpty)])-
polyvaln(fittemp,[x(midptx),y(midpty)]);
dtdx2=polyvaln(fittemp,[x(midptx),y(midpty)])-
polyvaln(fittemp,[x(midptx-1),y(midpty)]);

dtdy1=polyvaln(fittemp,[x(midptx),y(midpty+1)])-
polyvaln(fittemp,[x(midptx),y(midpty)]);
dtdy2=polyvaln(fittemp,[x(midptx),y(midpty)])-
polyvaln(fittemp,[x(midptx),y(midpty-1)]);

rate(1,3) = (dtdx1 + dtdx2)/(2*xinc);
rate(1,4) = (dtdy1 + dtdy2)/(2*yinc);

%%  Loop to Calculate all Layers

for count = 1:nlayers-2-2

clear lon lan temp height

%  Import Next Portion of .xls data file

lon = numeric((count*200)+1:(count*200)+200,1);
lat = numeric((count*200)+1:(count*200)+200,2);

temp = numeric((count*200)+1:(count*200)+200,4);
height = numeric((count*200)+1:(count*200)+200,5);

%%   Fit Surface to Temperatures for Lower Pressure Levels
fittemp = polyfitn...
    ([lon,lat],temp,'constant x y x^2 y^2 x^3 y^3');% x^4 y^4')

[ew, ns] = meshgrid(x,y);
tt = polyvaln(fittemp,[ew(:),ns(:)]);
tt = reshape(tt,yy,xx);

%%   Fit Surface to Heights for Lower Pressure Levels
fithgt = polyfitn...
    ([lon,lat],height,'constant x y x^2 y^2 x^3 y^3');% x^4 y^4')

[ew, ns] = meshgrid(x,y);
zz = polyvaln(fithgt,[ew(:),ns(:)]);
zz = reshape(zz,yy,xx);
```

```
%%   Plot Next Surface

%lowestcountour = floor(min(height)/50)*50; %Lowest Geopotential Height
lowestcountour = floor(min(temp));  %Lowest level for temperature
j=lowestcountour:countourspacing:lowestcountour+(contours*countourspaci
ng);

subplot(5,5,count+1)
title(['PressLayer = ',int2str(count), ' mb']);

%[C,h] = contour(ew,ns,zz,j);  %Plot height contours
[C,h] = contour(ew,ns,tt,j);  %Plot temp surfaces

clabel(C,h)
title([int2str(plevels(count+1)),' mb'])

%%  Calculating Rates of Height Change at DZ Coordinates

dhdx1=polyvaln(fithgt,[x(midptx+1),y(midpty)])-
polyvaln(fithgt,[x(midptx),y(midpty)]);
dhdx2=polyvaln(fithgt,[x(midptx),y(midpty)])-polyvaln(fithgt,[x(midptx-
1),y(midpty)]);

dhdy1=polyvaln(fithgt,[x(midptx),y(midpty+1)])-
polyvaln(fithgt,[x(midptx),y(midpty)]);
dhdy2=polyvaln(fithgt,[x(midptx),y(midpty)])-
polyvaln(fithgt,[x(midptx),y(midpty-1)]);

rate(count+1,1) = (dhdx1 + dhdx2)/2*(1/xinc);
rate(count+1,2) = (dhdy1 + dhdy2)/2*(1/yinc);

%%   Calculating Rates of Temp Change at DZ Coordinates

dtdx1=polyvaln(fittemp,[x(midptx+1),y(midpty)])-
polyvaln(fittemp,[x(midptx),y(midpty)]);
dtdx2=polyvaln(fittemp,[x(midptx),y(midpty)])-
polyvaln(fittemp,[x(midptx-1),y(midpty)]);

dtdy1=polyvaln(fittemp,[x(midptx),y(midpty+1)])-
polyvaln(fittemp,[x(midptx),y(midpty)]);
dtdy2=polyvaln(fittemp,[x(midptx),y(midpty)])-
polyvaln(fittemp,[x(midptx),y(midpty-1)]);

rate(count+1,3) = (dtdx1 + dtdx2)/2*(1/xinc);
rate(count+1,4) = (dtdy1 + dtdy2)/2*(1/yinc);

end

csvwrite('rate.csv',rate)  %Create table with temp/hgt slopes by layer
```

Appendix C: Additional RAOB Comparisons

Trapani, Italy, 12Z, 3 Jan, 2010

Geostrphic Wind:

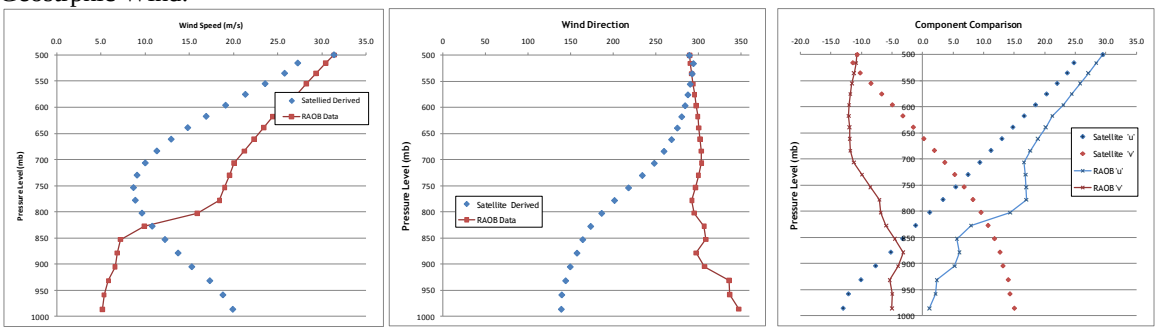

Thermal Wind:

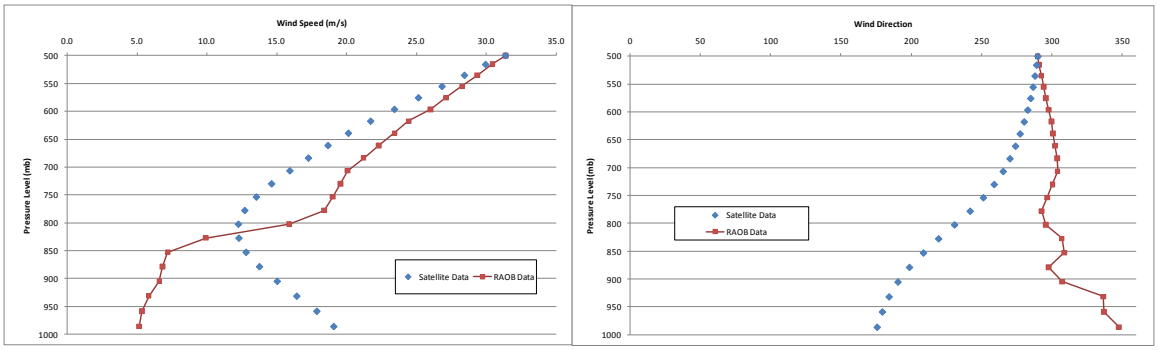

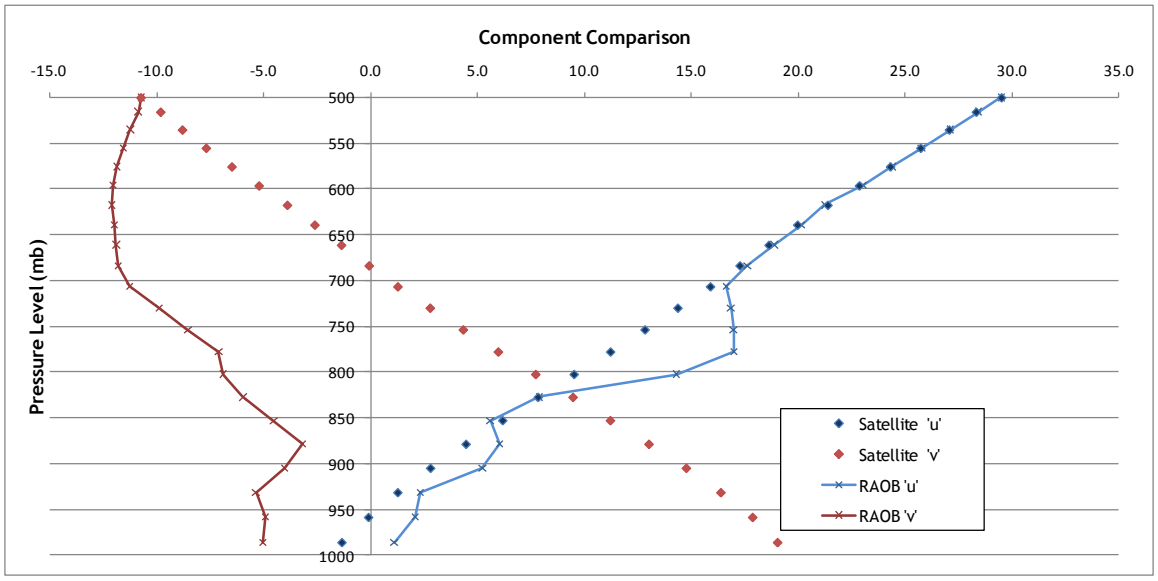

Oakland, CA, 3 Dec 09, 12Z

Calculated from 500mb level down:

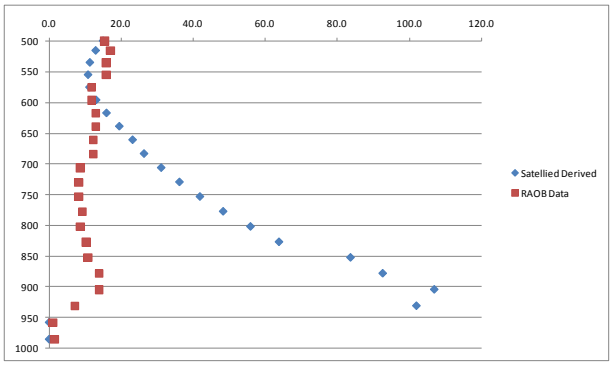

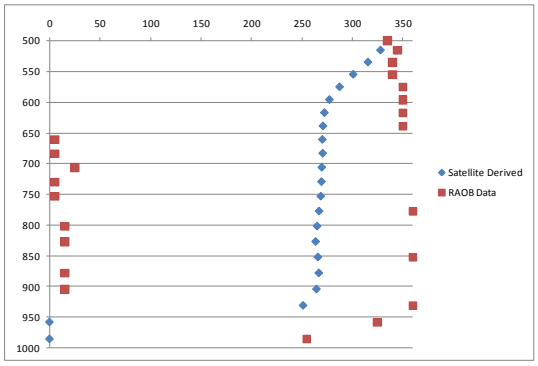

Calculated from surface level up:

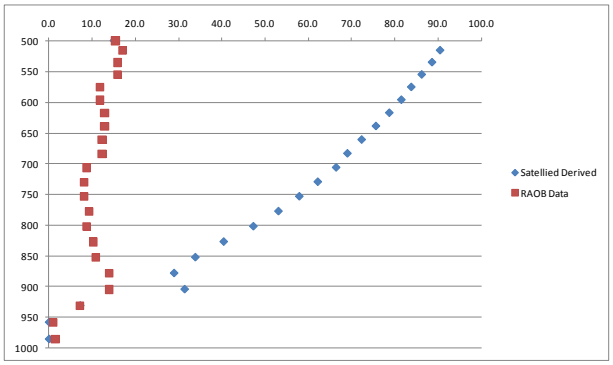

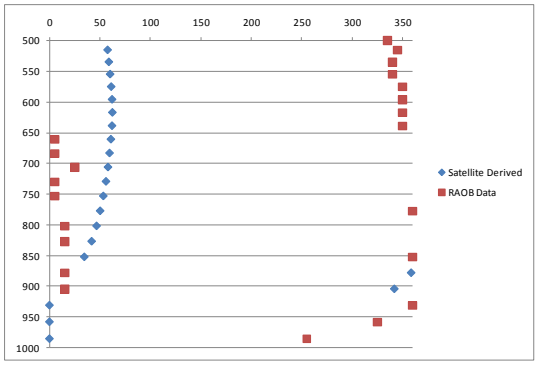

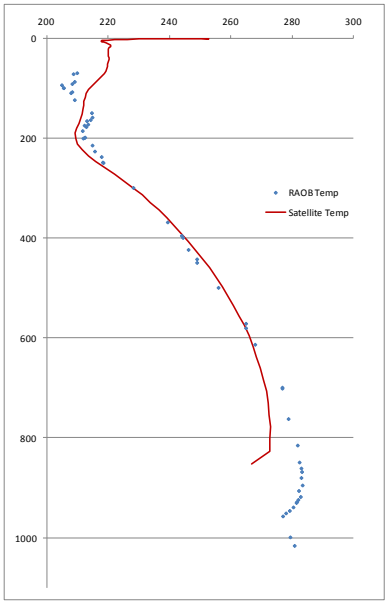

Stuttgart, Germany, 2 Dec 09, 12Z

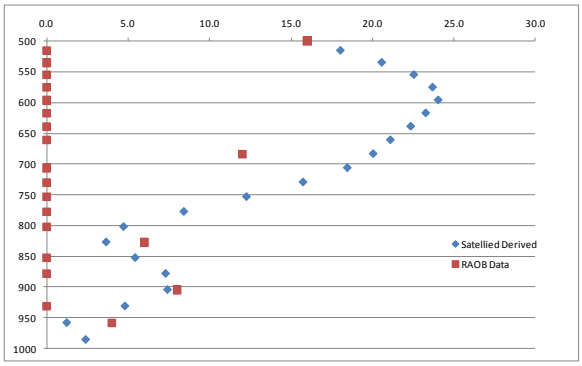
0.0
5.0
10.0
15.0
20.0
25.0
30.0
500
550
600
650
700
750
800
850
900
950
1000
Satellied Derived
RAOB Data

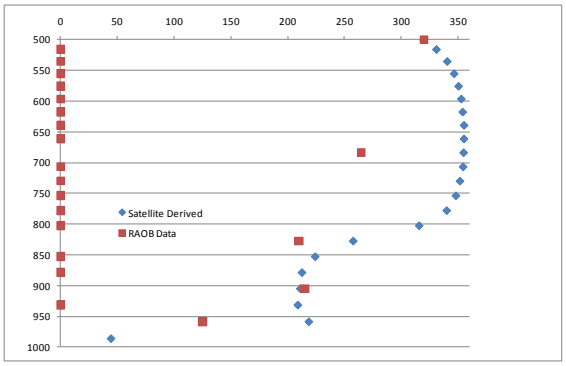
0
50
100
150
200
250
300
350
500
550
600
650
700
750
800
850
900
950
1000
Satellite Derived
RAOB Data

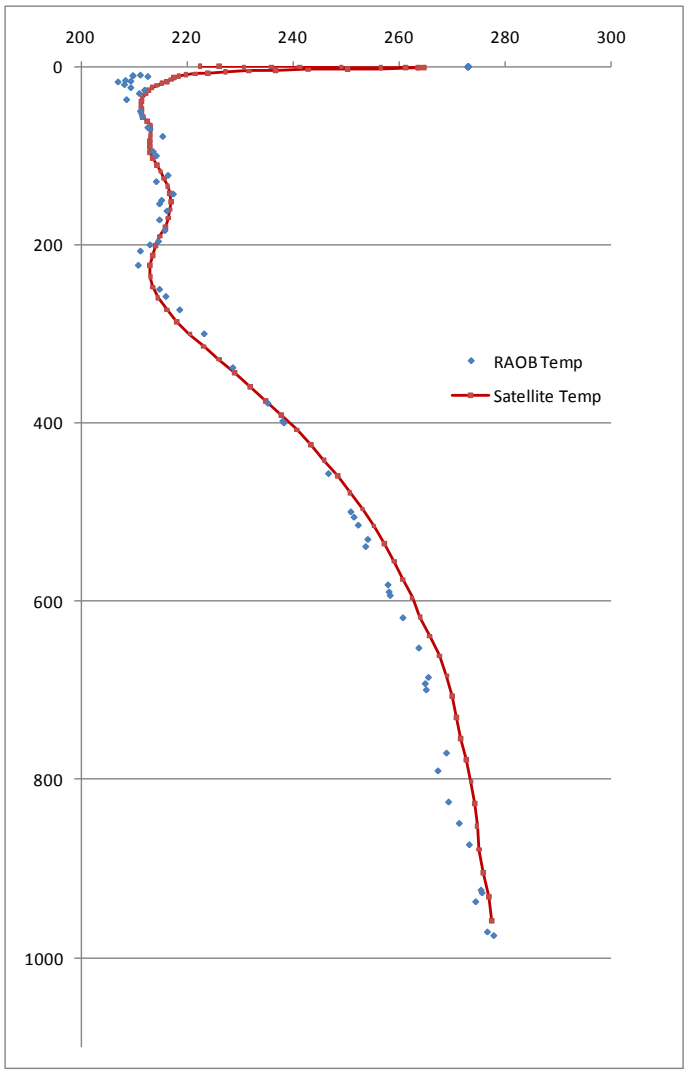
200
220
240
260
280
300
0
200
400
600
800
1000
RAOB Temp
Satellite Temp

Kauai, Hawaii, 3 Dec 09, 00Z

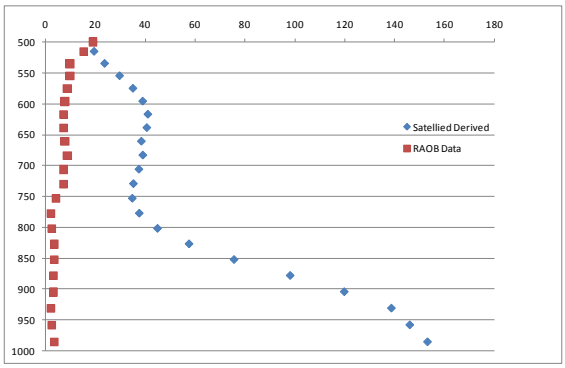

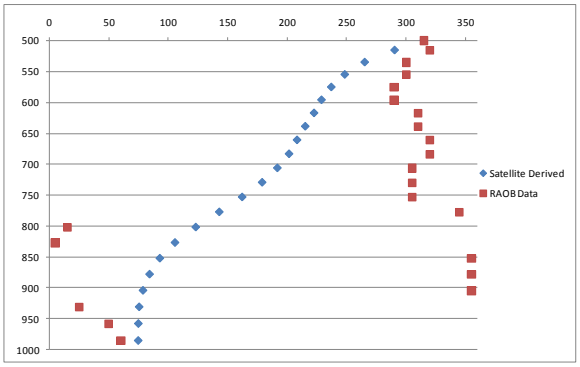

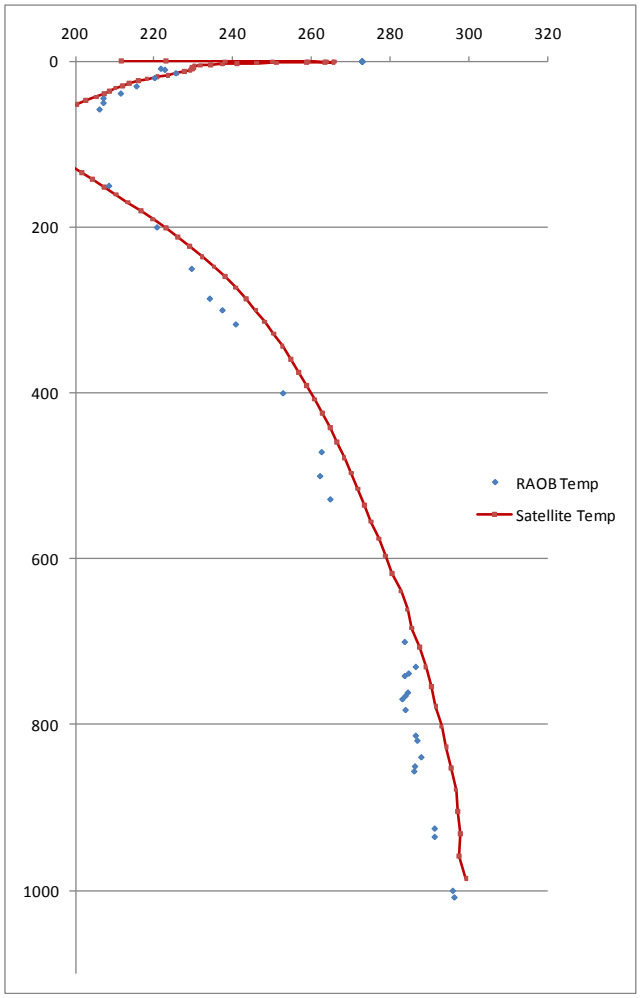

Fairbanks, AK, 25 Nov 09, 12Z

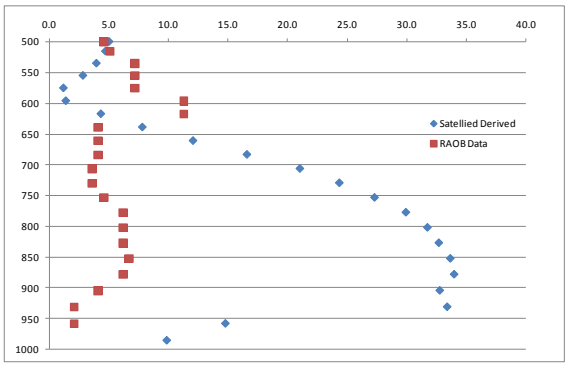

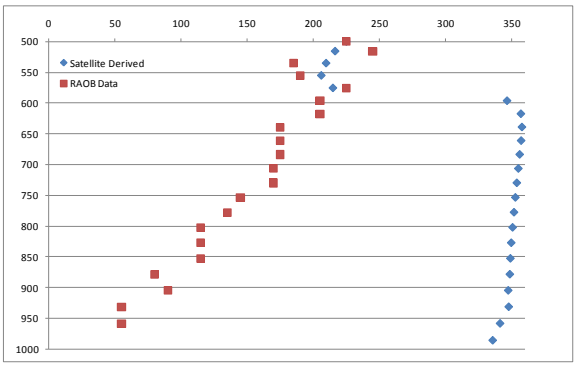

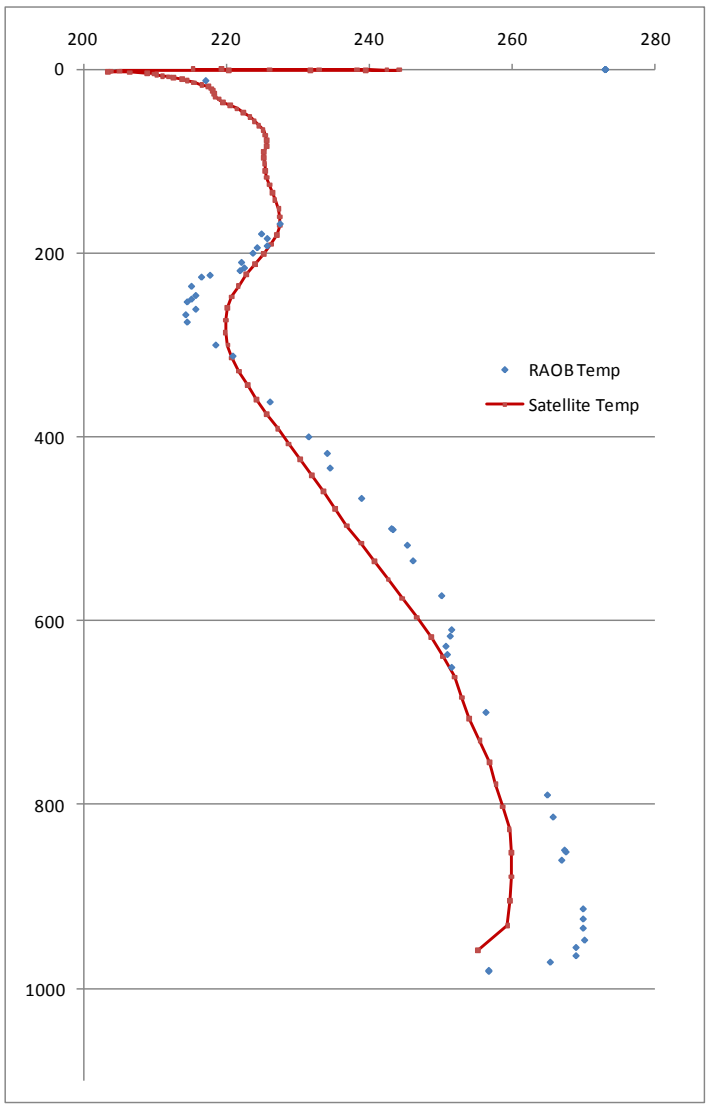

Bibliography

Air Force Weather Agency. *Joint Air Force & Army Weather Information Network (JAAWIN).* [On Line] Available: https://weather.afwa.af.mil/jaawin/specialsupport/specialsupport.jsp

AMC Single Pass Airdrop Workshop, *JPADS Background Paper*. HQ AMC. June 2009.

BAE Systems, *Atmospheric Infrared Sounder (AIRS).* [On Line] 2010. [Cited: October 25, 2009.] http://www.baesystems.com/ProductsServices/bae_prod_s2_airs.html

Benney, Richard J, *The New Military Applications of Precision Airdrop Systems*. American Institute of Aeronautics and Astronautics (AIAA) 2005-7069, 2005.

Bluestein, Howard B, *Synoptic-Dynamic Meteorology in Midlatitudes*, volume 1.New York: Oxford University Press, 1992.

Capewell, *Precision Air Drop System.* Company Brochure. Capewell Life Support/Aerial Delivery Systems. http://www.capewell.com/products_aerial_Airdrop.php

Cooperative Institute for Research in the Atmosphere, *CIRA Annual Report 2004-2005*. Colorado State University, 2005.

Crevoisier, Cyril, Alain Chedin, and Noelle A. Scott. *AIRS channel selection for CO_2 and other trace-gas retrievals.* Q. J. R. Meteorol. Soc. (2003), **129**. pp.2719-2740.

Department of the Air Force. Flying Operations, Computed Air Release Point Procedures. AFI 11-231, 31 July 2005. [On Line]. Available: http://afpubs.hq.af.mil

Department of the Air Force. Flying Operations, C-17 Operations Procedures. AFI 11-2C-117 Volume 3, 15 December 2005. [On Line]. Available: http://afpubs.hq.af.mil

Department of the Air Force. Flying Operations, C-130 Aircrew Training. AFI 11-2C-130 Volume 1, 19 July 2006. [On Line]. Available: http://afpubs.hq.af.mil

Department of the Air Force. Flying Operations, C-130 Operations Procedures. AFI 11-2C-130 Volume 3, 14 March 2006. [On Line]. Available: http://afpubs.hq.af.mil

EUMETSAT. *Monitoring Weather and Climate from Space-Press Release.* May 31, 2007 [On Line] Available: http://www.eumetsat.int/Home/Main/News/Press_Releases/029837?l=en

European Space Agency. *Monitoring the Weather from Polar Orbit. BR-261* Brochure. EAS Publications Division, Noordwijk, The Netherlands. May 2006

Fujiwara, M, M. Ondras, H. Vomel, J. Wang, J. Nash, D. Seidel, and P. Thorne. *Specifications for a Reference Radiosonde for the GCOS Reference Upper-Air Network (GRAUN).* Working Group on Atmospheric Reference Observations. July-October 2008.

Gemas, David L. *A Systems Engineering Approach to Analyzing Weather Input Sensitivites of the Joint Precision Air Drop System.* Wright-Patterson AFB: Air Force Institute of Technology., March 2007.

Hattis, Philip, Kai Angemueller, Thomas Fill, Robert Wright, Richard Benney, and David LeMoine. *An In-flight Precision Airdrop System.* Draper Laboratory, Cambridge, MA., 2006.

Headquarters Air Mobility Command, *MAF JPADS CONEMP*. HQ AMC/A3D, 18 June 2009.

Holton, James R. *An Introduction to Dynamic Meteorology*. Academic Press, San Diego, CA, 1979.

Jet Propulsion Laboratory, *AIRS Version 5.0 Released Files Description.* California Institute of Technology, July 2007.

Jet Propulsion Laboratory, *AIRS* Animation. [On Line]. Available: http://photojournal.jpl.nasa.gov/animation/PIA11170 .

Jet Propulsion Laboratory, *How AIRS Works, Detailed Desctiption*. [On Line] Available: http://airs.jpl.nasa.gov/technology/how_AIRS_works/how_AIRS_works_detail/

JPADS Mission Planner. Version 5.1.0, Computer Software, Planning Systems, Inc.C.S. Draper Laboratory, 2006.

Kidder, Stanley Q. and Vonder Haar, Thomas H., *Satellite Meteorology*. San Diego: Academic Press, Inc, 1995.

Ma, Xia L., Timothy J. Schmit and William L. Smith, 1999: A Nonlinear Physical Retrieval Algorithm. *American Meteorological Society*, **38**, 500-513.

Menzel, W. Paul, Frances C. Holt, Timothy, J. Schmit, Robert M. Aune, Anthony J. Schreiner, Gary S. Wade and Donald G. Gray. *Application of GOES-8/9 Soundings to Weather Forecasting and Nowcasting*, 1998.

MetEd-The COMET Program. *Numerical Weather Prediction-GFS Introduction.* [On Line] May 2007. Available: http://www.meted.ucar.edu/nwp/pcu2/avintro.htm

NASA, *Earth Observatory-Three Classes of Orbit***.** [On Line] Available: http://earthobservatory.nasa.gov/Features/OrbitsCatalog/page2.php

NASA, *Satellite Overpass Predictor***.** [On Line] Available: http://earthobservatory.nasa.gov/MissionControl/overpass.php

Olander, Timothy L., *UW-CIMSS Satellite-Derived Wind Algorithm User's Guide.* Cooperative Institute for Meteorological Satellite Studies - Space Science and Engineering Center, University of Wisconsin—Madison, 2001.

Petty, Grant W., *A First Course in Atmospheric Radiation* (2nd Edition). - Madison : Sundog Publishing, 2006.

QinetiQ-North America, *PADS-Precision AirDrop System.* [On Line] 2008. Available: http://www.planningsystemsinc.com/downloads/DS08_083_PADS%20w_generic_c.pdf

Sela, J., 1980: Spectral modeling at the National Meteorological Center. *Mon. Wea. Rev.*, 1**08**, 1279-1292

Staine-Pyne, Erin, Major, USAF. *AMC Industry Days Briefing.* Headquarters Air Mobility Command, 28 April 2009.

Sterner, Ray, *Southcentral Alaska Topographic Map.* Johns Hopkins University Physics Laboratory, 1997. [On Line] Available: http://fermi.jhuapl.edu/states/maps1/ak_sc.gif

University of Virginia, Department of Environmental Sciences. Atmosphere and Weather course materials. 2010. [OnLine] Available: http://www.evsc.virginia.edu/~evscta/EVSC350/overheadsIII/9.jpg

Wallace, John M. and Hobbs, Peter V. *Atmospheric Science, An Introductory Survey* (2nd Edition). Amsterdam: Academic Press, 2006.

WebMET.com. *Radiosonde Sounding System.* [On Line]. 2002. Available: http://www.webmet.com/met_monitoring/912.html

Wuest, Michael R. and Richard J. Benney., *Precision Airdrop*. NASA Center for AeroSpace Information (CASI). 2005

Zonum Solutions. *Free Software Tools-E-Query Elevation Extraction.* [On Line] 2007. Available: http://www.zonums.com/online/equery.html

Zou, C.Z., and M.L. Van Woert, 2002: *Atmospheric Wind Retrievals from Satellite Soundings over the Middle- and High-Latitude Oceans*. *Mon. Wea. Rev.*, **130**, 1771–1791.

REPORT DOCUMENTATION PAGE	Form Approved OMB No. 074-0188

1. REPORT DATE *(DD-MM-YYYY)*	**2. REPORT TYPE**	**3. DATES COVERED** *(From – To)*
25 -03-2010	Master's Thesis	Jan 2009 - Mar 2010

4. TITLE AND SUBTITLE

Application of Satellite-Derived Wind Profiles to Joint Precision Airdrop System (JPADS) Operations

5a. CONTRACT NUMBER

5b. GRANT NUMBER

5c. PROGRAM ELEMENT NUMBER

6. AUTHOR(S)

Meier, David C., Maj, USAF

5d. PROJECT NUMBER

5e. TASK NUMBER

5f. WORK UNIT NUMBER

7. PERFORMING ORGANIZATION NAMES(S) AND ADDRESS(S)

Air Force Institute of Technology
Graduate School of Engineering and Management (AFIT/EN)
2950 Hobson Way
WPAFB OH 45433-7765

8. PERFORMING ORGANIZATION REPORT NUMBER

AFIT/GAP/ENP/10-M10

9. SPONSORING/MONITORING AGENCY NAME(S) AND ADDRESS(ES)

Detachment 3, 16 WS
2049 Monahan Way, Area B, Bldg 91
Wright-Patterson AFB, OH 45433

516th AESW/XR
2590 Loop Rd West, Area B, Bldg 558
Wright-Patterson AFB, OH 45433

10. SPONSOR/MONITOR'S ACRONYM(S)

Det3 16WS, 516 AESW/XR

11. SPONSOR/MONITOR'S REPORT NUMBER(S)

12. DISTRIBUTION/AVAILABILITY STATEMENT

APPROVED FOR PUBLIC RELEASE; DISTRIBUTION UNLIMITED.

13. SUPPLEMENTARY NOTES

14. ABSTRACT

The Joint Precision Airdrop System has revolutionized military airdrop capability, allowing accurate delivery of equipment and supplies to smaller drop zones, from higher altitudes than was previously possible. This capability depends on accurate wind data which is currently provided by a combination of high-resolution forecast models and GPS dropsondes released in the vicinity of the dropzone shortly before the airdrop. This research develops a windprofiling algorithm to derive the needed wind data from passive IR satellite soundings, eliminating the requirement for a hazardous dropsonde pass near the drop zone, or allowing the dropsonde to be dropped farther from the dropzone. Atmospheric temperature measurements made by the Atmospheric Infrared Sounder (AIRS) onboard the polar-orbiting Aqua satellite are gridded and filtered to create a three-dimensional temperature field surrounding a notional airdrop objective area. From these temperatures, pressure surfaces are calculated and geostrophic and thermal wind direction and magnitude are predicted for 25 altitudes between the surface and 500 mb level. These wind profiles are compared to rawinsonde measurements from balloon releases near the notional airdrop location and time of the satellite sounding. The validity of the satellite-derived wind profile is demonstrated at higher altitudes, but this method does not consistently predict wind velocity within the boundary layer. Future research which better accounts for surface friction may improve these results and lead to the single-pass airdrop capability desired by Air Mobility Command.

15. SUBJECT TERMS

16. SECURITY CLASSIFICATION OF:			**17. LIMITATION OF ABSTRACT**	**18. NUMBER OF PAGES**	**19a. NAME OF RESPONSIBLE PERSON**
REPORT	**ABSTRACT**	**c. THIS PAGE**			Dr. Steven T. Fiorino, (ENP)
U	**U**	**U**	**UU**	96	**19b. TELEPHONE NUMBER** *(Include area code)* (937) 255-6565, x4506 steven.fiorino@afit.edu

Standard Form 298 (Rev: 8-98)
Prescribed by ANSI Std. Z39-18